Reconciling ionic-transport properties with atomic structure in oxide glasses

G. N. Greaves
Council for the Central Laboratory, Daresbury Laboratory, Warrington WA4 4AD, United Kingdom

K. L. Ngai
Naval Research Laboratory, Washington, D.C. 20375-5000
(Received 22 November 1993; revised manuscript received 13 March 1995)

Structural evidence for the microsegregation of alkalis in oxide glasses is reviewed and the implications for ionic transport, viz., nearest-neighbor hopping, cooperative and correlation effects, are considered. Distinctions are drawn between the hopping of alkalis in silicate glasses, where changes in the configurations of neighboring bridging and nonbridging oxygens are expected, and alkali hopping in fully compensated aluminosilicate glasses where nonbridging oxygens are absent and conformational changes in the network are minimized. A simple expression is introduced for the microscopic energy barrier facing a migrating alkali E_a, and this is corrected to account for the cooperative effects of the other ions involved by dividing by the Kohlrausch exponent β, which defines the conductivity relaxation function $\exp[-(t/\tau^*)\beta]$. Structural parameters determined by x-ray and NMR spectroscopy enable us to calculate E_a. Conductivity relaxation experiments give a measure of β. The macroscopic diffusion enthalpy that is measured, W, is given by the ratio E_a/β. Thus we are able to show how the local structure of an alkali in a silicate glass can be used to predict the measured diffusion enthalpy. The smaller values of W reported for aluminosilicate glasses are rationalized structurally in terms of the removal of nonbridging oxygens from the modified network. In considering silicate glasses containing small concentrations x of alkali, as this necessarily leads to reductions in alkali microsegregation, decreased cooperative effects and increased hopping distances are expected. Taken together with the attendant fall in the high-frequency dielectric constant and the rise in β, this combination of changes naturally explains the increased enthalpies observed in low alkali glasses and the rise in alkali diffusion frequency factors. Increased hopping distances are also invoked to explain the crossover dependences of the diffusion coefficients and enthalpies of the separate alkalis in mixed alkali glasses. In particular, the increase in W for a given alkali, as its proportion γ drops for a fixed alkali concentration x, is attributed to an increase in the hopping distance and can again be predicted from the local structure, providing allowance is made for an associated reduction in cooperative effects. From the separate local structures of the two alkalis, the observed fall in the diffusion coefficients of the two alkalis and the minima in the isothermal dc electrical conductivity resulting from the increase in the respective diffusion enthalpies are well reproduced. In addition, the maxima in the measured dc electrical conductivity enthalpy W in the Kohlrausch exponent β and also in the Haven ratio f, all characteristic of alkali mixing, are closely predicted. Finally the increase in magnitude of the mixed alkali effect reported in aluminosilicate glasses is explained in terms of increased cooperativity associated with the reduced energy barriers E_a for the two alkalis resulting from there being fewer nonbridging oxygens present in the glass structure.

I. INTRODUCTION

At the atomic level the structure of an oxide glass is complex, both from an empirical and from a perceptual standpoint. Standard techniques like x-ray diffraction, while providing specific descriptions of nearest-neighbor geometries, yield only ambiguous structural information about interatomic distances of 5 Å and more. This underdetermination of glass structure frustrates the ambition to visualize the morphology resulting from atomic correlations beyond nearest and next-nearest neighbors. Generally referred to as intermediate-range order, this is the regime particularly relevant to ionic diffusion as it is over these distances that ions will interact and where cooperative phenomena, not least the mixed alkali effect,[1] will be played out. While the continuous random network (CRN) of Zachariasen[2] continues to provide a pragmatic solution for rationalizing well-defined short-range order with the absence of atomic periodicity, the process by which glass-forming bonds become partly depolymerized in a modified glass has, until recently, proved difficult to identify, let alone characterize.

Considerable advances in elucidating the structure of modified oxide glasses, however, have been made through the use of new techniques, notably x-ray-absorption fine-structure (XAFS) spectroscopy,[3–5] but also magic angle spinning NMR (MASNMR) (Refs. 6–9) isotopic substitution neutron scattering[10] as well as the traditional spectroscopies of IR,[11] Raman,[12] and x-ray photoemission spectroscopy (XPS).[13,14] Experimental findings from these studies have been corroborated by recent sophisticated molecular dynamics (MD) simulations,[15–18] all of

 ©1995 The American Physical Society

which reveal new intermediate-range order and microstructure characterized by the microsegregation of modifying components from the network-forming CRN. Accordingly, for alkali silicates, the alkalis form clusters, and at glass-forming compositions, these join to create channels in a modified random network (MRN).[19] Microstructure in crystalline silicates is well known, manifest in the silicate chains and layers of corner-sharing tetrahedra. The MRN extends this architecture in the context of disordered topology. Long-range disorder is meted out primarily through bond angle variations, leaving short-range order invariant and reflecting the dominant chemical interactions between atoms.

As well as offering a fruitful way of simplifying complexities in the structure of silicate glasses, the MRN also provides a way of visualizing ionic transport in which the mobile alkalis travel through the glass, primarily along the alkali-rich sublattice.[19] As the alkali concentration falls, though, these pathways cease to be continuous, and below the percolation threshold, ionic transport is expected to revert to the network. Taking these extreme situations as starting points, the Coulombic interactions and conformational changes associated with the hopping of alkalis can be described in terms of the local atomic structure. Simple expressions for the diffusion enthalpy of an alkali, which can be readily parametrized from the results of spectroscopies like XAFS, MASNMR and IR, have been proposed and the MRN concept exploited to accurately predict the ionic transport properties sodium silicate glasses as a function of alkali concentration x.[20] In this paper these ideas and preliminary results are extended to cover potassium silicate glasses, the variations in transport properties resulting from different concentrations of these alkalis in mixed-alkali silicate glasses. In addition, the associated changes in ionic transport in aluminosilicate glasses will also be considered, in particular the effect of varying the proportions of alumina to alkali oxide. As a result, we are now able to quantitatively predict the major phenomena in ionic transport exhibited by a wide range of oxide glasses simply from a knowledge of the atomic environments of the alkalis present.

II. RANDOM NETWORKS

We begin by making the standard distinction between bridging oxygens (BO's) coordinated to two silicons and nonbridging oxygens (NBO's) coordinated to only one silicon. This is important because the type of oxygen to which *alkalis* are coordinated is crucial in specifying the possible *network processes* involved in ionic transport. Figure 1 contrasts two extreme types of random network constructed to represent alkali oxide glasses, one incorporating both BO's and NBO's [Fig. 1(a)] and the other only BO's [Fig. 1(b)]. The types of atoms and bonds are given in the key to the figure. In the MRN shown in Fig. 1(a), which comprises both types of oxygen, alkalis are shown only coordinated to NBO's. Moreover, modifying cations, NBO's, network-forming cations, and BO's are all consistently coordinated, NBO's primarily to alkalis and BO's to silicons. Percolation pathways for migrating modifying cations can be mapped out by connecting NBO's together, thereby identifying the boundaries of the conducting channels. Further details of the MRN can be found elsewhere.[19]

The other network illustrated in Fig. 1(b) is constructed to represent an aluminosilicate glass for which R (the molar ratio Al_2O_3/M_2O) is equal to 1. By analogy with crystalline feldspar structures which contain no NBO's, the vast majority of oxygens in $R=1$ glasses should be in BO configurations. For clarity the random network presented in Fig. 1(b) contains no NBO's. Furthermore, all aluminums are shown occupying network-forming sites equal in number to the "network-modifying" alkalis. Accordingly, there is a new type of oxygen: a BO coordinated to an alkali in addition to two silicons. Alkalis are only coordinated to this kind of oxygen. As a result of these new coordination rules, the alkali aluminosilicate network shown in Fig. 1(b) is topologically similar to a Zachariasen CRN. On the other hand, because alkalis and aluminums are present in equal quantities, the charge on each alkali ion M^+ is balanced by the charge on each AlO_4^- group. Figure 1(b) therefore represents a "compensated" continuous random network (CCRN). The distribution of alkalis in Fig. 1(b), however, is not homogeneous. This is because alkalis are strictly coordinated and associated with aluminate groups via threefold BO's. As a result of this, the CCRN microsegregates in a similar way to the MRN. In recent MD calculations evidence for clustering of AlO_4^- groups and alkalis has been found in simulated threedimensional structures.[21] Just as the MRN can be subdivided into two sublattices via NBO's, so can the threefold BO's be used to divide the CCRN into alkali-rich and alkali-rare regions. Once again transport is predicted to occur predominantly along those pathways where alkalis (and also AlO_4^-'s) are microsegregated.

For aluminosilicate compositions for which $0<R<1$, we envisage random network structures intermediate between the MRN and CCRN. Ionic transport should again follow alkali-rich routes, but in some regions these will be prescribed by NBO's and in others by AlO_4^-'s.

For the MRN, CCRN, and intermediate structures, the proximity of other alkalis in silicate and in aluminosilicate glasses will lower the Coulomb barrier facing the diffusion of a single alkali. This will encourage transport in the presence of other alkalis as we have envisaged above, but by default will draw in cooperative phenomena which will slow ionic diffusion down.[22] We have already shown how these effects can be reconciled in sodium silicate glasses and how the activation energy for ionic diffusion—in particular its dependence on alkali concentration—can be reproduced from a knowledge of the local structure.[20] The same ideas, suitably modified by clues given by the two types of network presented in Fig. 1, can also provide a quantitative description of the relationships between structure and transport in both compensated ($R=1$) and uncompensated ($0<R<1$) aluminosilicate glasses.

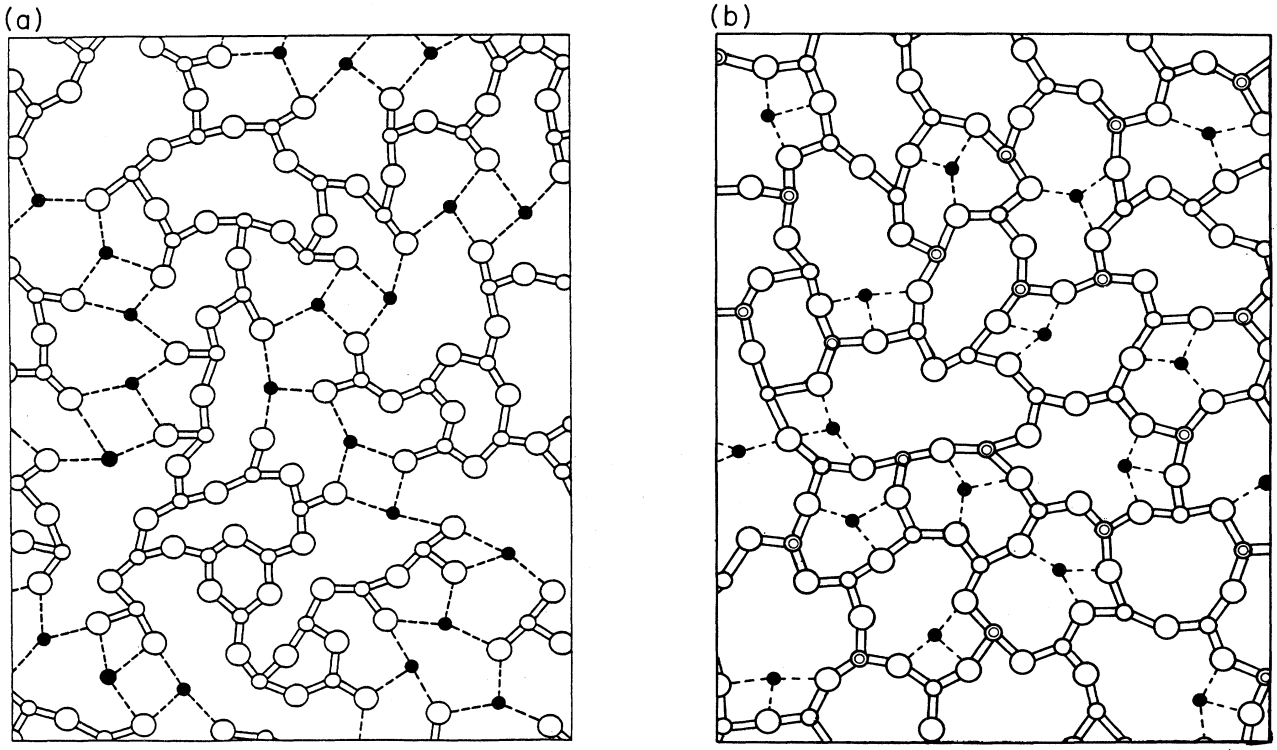

FIG. 1. Random network models for oxide glasses. Oxygens are shown by the large open circles and silicons by the small open circles with aluminums by the small double circles. The solid circles represent modifying cations like alkalis. The directional bonds comprising the network are indicated by solid lines and the ionic bonds of the modifying component by dashed lines. (a) MRN for silicate glasses (Ref. 19). Modifying cations are predominantly coordinated to NBO's and vice versa. Apart from BO's, all atoms are strictly threefold coordinated for this two-dimensional network. (b) CCRN for $R=1$ aluminosilicate glasses. Modifying cations are coordinated to BO's and charge compensated by aluminate groups. With the exception of network BO's, all atoms are threefold coordinated. Note that in both networks there is evidence for the microsegregation of glass modifiers from glass formers.

III. MICROSEGREGATION IN OXIDE GLASSES

Microsegregation in oxide glasses is the common characteristic of all recent MD simulations.[15–18,21] It can be detected in the partial radial distribution functions (RDF's) of the alkalis. Experimental evidence for alkali clustering in silicate and aluminosilicate glasses can be seen in Fig. 2, which shows the atomic distribution of sodium in a silicate glass ($Na_2Si_4O_9$) and in an aluminosilicate glass ($Na_{0.17}Al_{0.03}Si_{0.23}O_{0.56}$) obtained from sodium K-edge XAFS experiments.[5,20] The main peak close to 2.3 Å is due to nearest-neighbor oxygens, but there is also a weaker second peak between 3 and 4 Å which can be attributed to neighboring sodiums and silicons, consistent with the clustering of alkalis in these glasses. In particular, for $Na_2Si_4O_9$ glass, for which the second peak is strongest, Na-Na distances have been refined at 3.2 Å with sodium-silicon distances at 3.8 Å. For the aluminosilicate glass both these distances are closer to 4 Å. The detection of a second coordination shell using XAFS that can be attributed to alkali-alkali distances has also been reported for potassium and caesium silicates.[23] The distances are longer than for sodium silicates, scaling with the size of the alkali. The statistical alkali-alkali separation $2(3/4\pi N)^{1/3}$ can be estimated from the atomic concentration N and is between 5 and 6 Å for alkali disilicate glasses. In all cases this is significantly greater than the $R_{M\text{-}M}$ values recorded from alkali XAFS experiments like those shown in Fig. 2(a) or indeed from MD simulations[17] and confirms the clustering of alkalis in oxide glasses.

Microsegregation in oxide glasses was originally speculated on the basis of the well-defined local environments of network-modifying and network-forming cations detected with XAFS.[19] The oxygen coordination number for sodium in the $Na_2Si_4O_9$ glass shown in Fig. 3 is 4.(3) and the Debye-Waller factor, $2\sigma^2$, 0.017 Å^2. In particular, the Debye-Waller factor is predominantly thermal in origin, signifying sodium environments for the glass with little or no site-to-site variability. If, as we have previously argued,[3,4,19] the oxygens coordinated to alkalis in silicate glasses are chiefly NBO's, then charge balance and bond consistency demand equivalent cation configurations for NBO's. This complementarity of alkali and NBO configurations occurs in crystalline silicates, and so it should not be so surprising if the same arrangements were not also reflected in the short-range order of alkalis and oxygens in silicate glasses. In particular, in crystalline silicates like $Na_2Si_2O_5$ NBO's are coordinated to four alkalis and to one silicon. Novel ^{17}O NMR experiments on binary silicate glasses indicate that

NBO's indeed are highly coordinated to alkalis.[9] If alkalis are predominantly coordinated to NBO's and NBO's mainly to alkalis, then the microsegregation of alkalis from the network via intervening NBO's is inevitable.

Spectroscopic experiments on aluminosilicate glasses to establish whether equivalent microstructure exists here as in silicate glasses are currently in progress, but some differences are expected. In particular, it is clear from Fig. 2 that the alkali environment is altered when alumina is present in a silicate glass. Compared to $Na_2Si_4O_9$ glass, the coordination number of oxygens around sodium in $Na_{0.17}Al_{0.03}Si_{0.23}O_{0.56}$ glass falls to 2.(8) and the Debye-Waller factor increases to 0.024 Å^2. This can be clearly seen in the correlation maps presented in Fig. 2. These indicate the contours of equal significance in least-squares fitting of XAFS to a single shell of oxygens and are easily distinguished for the two glasses. We can understand these changes qualitatively with reference to the networks in Fig. 1 where it is not difficult to see how modifiers are more likely to exist in a variety of sites in a compensated aluminosilicate network for which there are two different network formers and no terminal oxygens than in a silicate structure moderated by NBO's. Clustering of alkalis will almost certainly ensue if modifiers

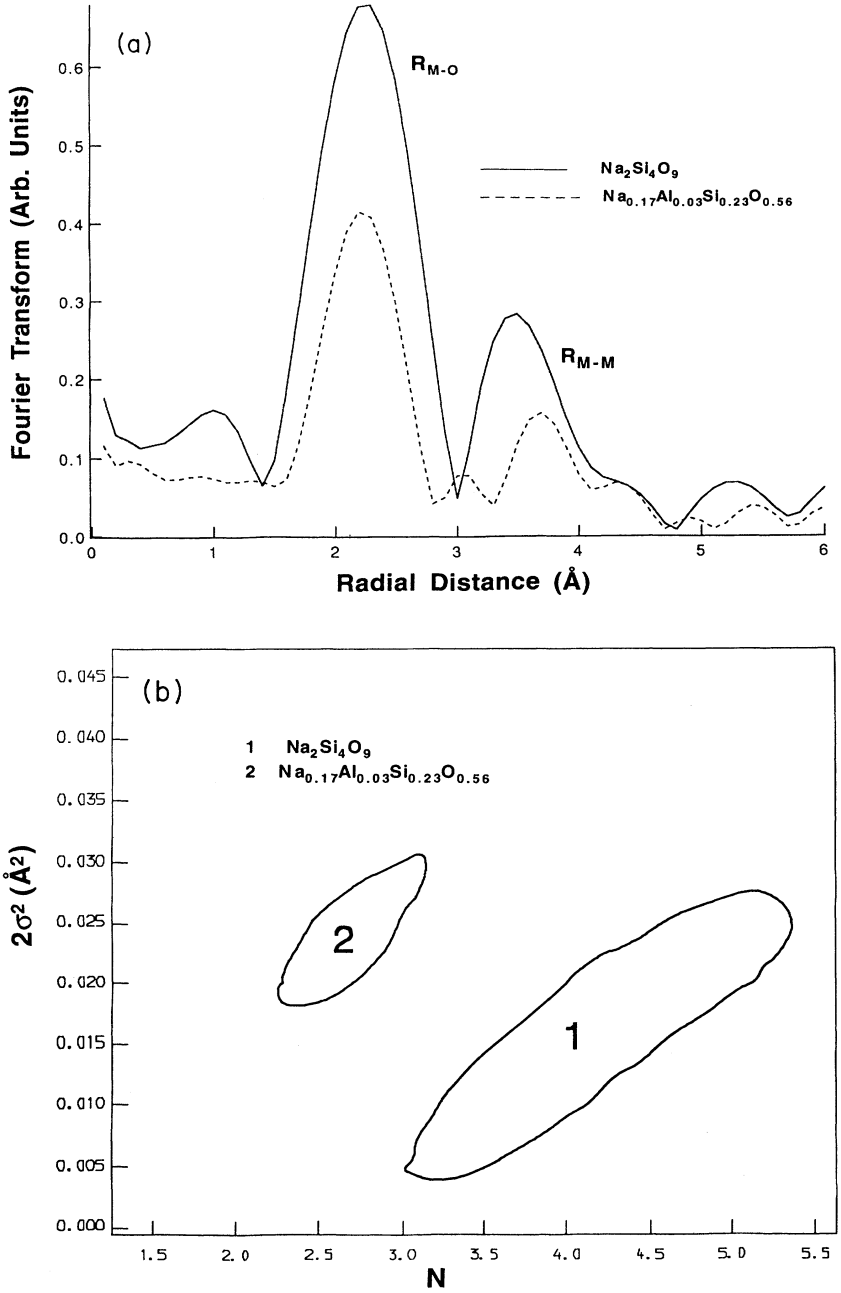

FIG. 2. Partial RDF's for sodium in two oxide glasses (Refs. 5,20). Fourier transforms of sodium K-edge XAFS are shown in the upper frame. $R_{M\text{-}O}$ and $R_{M\text{-}M}$ indicate sodium-oxygen and sodium-cation correlations, respectively. The solid curve refers to $Na_2Si_4O_9$ glass and the dashed curve to $Na_{0.17}Al_{0.03}Si_{0.23}O_{0.56}$ glass. The lower frame displays Debye-Waller ($2\sigma^2$) versus coordination number (N) correlation maps. 95% significance contours clearly distinguish the sodium sites in the two glasses.

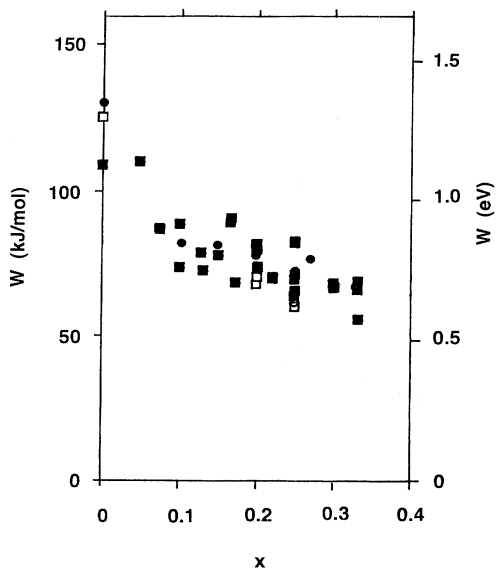

FIG. 3. Diffusion activation enthalpy values W plotted as a function of composition x in binary $[Na_2O]_x[SiO_2]_{1-x}$ (■) and $[K_2O]_x[SiO_2]_{1-x}$ glasses (●) (Ref. 24). Open symbols refer to dc electrical conductivity activation enthalpies (Ref. 22).

are preferentially coordinated to AlO_4^- tetrahedra as MD calculations demonstrate,[21] but this has yet to be directly confirmed spectroscopically.

IV. COULOMB BARRIERS FACING MIGRATING ALKALIS

We have seen in Fig. 2 how the alkali-oxygen radius $R_{M\text{-}O}$ and the alkali-alkali distance $R_{M\text{-}M}$ can be obtained directly from XAFS spectroscopy measured at the relevant alkali absorption edge. The electrostatic binding energy of the alkali, E_b, can be written simply as

$$E_b = e^2/4\pi\varepsilon_0\varepsilon_{hf}[1/R_{M\text{-}O}] . \quad (1)$$

The alkali cation is presumed to be fully charged, and the depth of the Coulomb well is therefore governed by the alkali-oxygen radius $R_{M\text{-}O}$ and ε_{hf}, the high-frequency dielectric constant. ε_0 is the permittivity of free space. The appropriate frequencies for ε_{hf} are typically in the rf to microwave range for oxide glasses. Generally, at frequencies above 10^5 Hz and at temperatures below the glass transition temperature T_g, there is little or no dispersion in the electrical conductivity and ε_{hf} relates to the dielectric response in the immediate vicinity of the alkali. For silica ε_{hf} is 4.5, and for a Na-O distance of 2.3 Å the binding energy of an isolated sodium cation in this glass is 1.38 eV, which is close to the activation energy for sodium diffusion at impurity loadings. For isolated potassium cations in silica with $R_{K\text{-}O}$ equal to 2.6 Å, $E_b = 1.24$ eV. The measured diffusion enthalpies W reported[24] for sodium (■) and potassium (●) in binary silicate glasses $(M_2O)_x(SiO_2)_{1-x}$ [M=Na, K] are plotted in Fig. 3. Although there is considerable scatter in these results from different groups (probably relating to different degrees of phase separation), enthalpies clearly originate

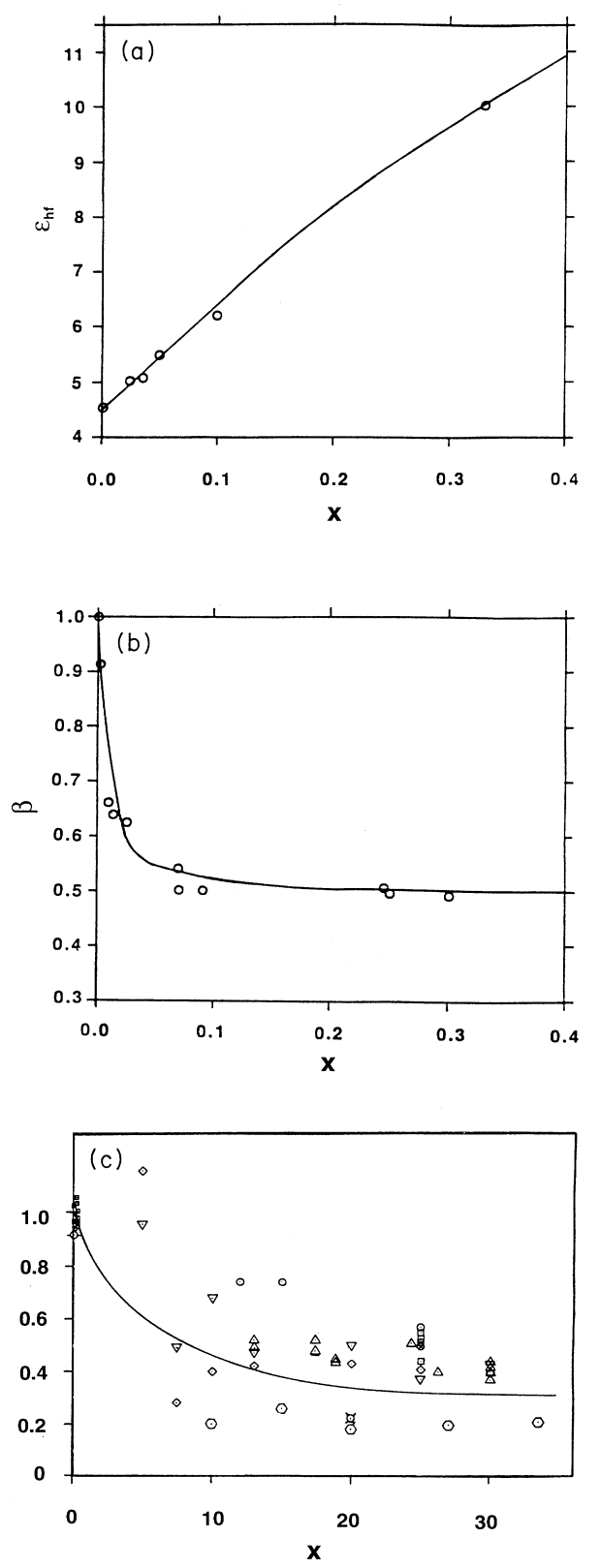

FIG. 4. Variations in the (a) high-frequency dielectric constant ε_{hf}, (b) the Kohlrausch coefficient β, and (c) the Haven ratio f with alkali concentration x reported for oxide glasses (Refs. 20,22,25,45).

at values of between 1.2 and 1.3 eV for low concentrations of alkali.

As the alkali concentration x increases, the empirical enthalpies cataloged in Fig. 3 demonstrate a systematic decrease, leveling out to reach values of around 0.6 eV by the time the disilicate composition ($x=\frac{1}{3}$) is reached. For all but the most dilute glasses, the Coulomb barrier facing a mobile alkali will be considerably less than E_b given by Eq. (1), being reduced by increases in ε_{hf} with composition and by reductions in the average hopping distance. The rise in ε_{hf} values with x for binary sodium silicates is shown in Fig. 4(a).[20,25] It is not immediately obvious how the average hopping distance can be measured. At T_g and above, however, alkalis are in considerable motion. If we assume that the ionic conduction mechanisms in the glass are an extension of this behavior, but with a far more rigid network, it is then reasonable to equate the frozen-in interalkali distance $R_{M\text{-}M}$ with the average hopping distance of the alkali in the glass. Accordingly, the Coulomb barrier facing a mobile alkali in a concentrated glass will be lowered from E_b to

$$e^2/4\pi\varepsilon_0\varepsilon_{hf}[1/R_{M\text{-}O}-1/R_{M\text{-}M}] .$$

For stable silicate compositions, ε_{hf} is typically ~ 10 [Fig. 4(a)]. Taking the $R_{M\text{-}O}$ and $R_{M\text{-}M}$ distances for sodium and potassium directly from XAFS, we obtain Coulomb barrier heights of $\sim 0.1-0.2$ eV. These values, however, are only a small fraction of the measured activation energy for alkali diffusion in silicate or in aluminosilicate glasses,[24] which are typically around 0.6 eV for stable single-alkali compositions as we have seen in Fig. 3.

Clearly the Coulomb barrier calculated from the local structure of the alkali matches the measured diffusion activation enthalpy for isolated alkalis in dilute quantities, but seriously underestimates it for alkalis at the concentrations usually encountered in stable oxide glasses, suggesting many-body effects may be involved. We have already presented strong evidence for alkali microsegregation from glass structure experiments. We will now explore the consequences of this on ionic transport in both alkali silicate and alkali aluminosilicate glasses.

V. HOPPING MECHANISMS

The coordination of modifying cations to NBO's or BO's will result in two types of alkali hopping, which we differentiate according to the extent to which the network reconfigures in the hopping process. These are both sketched in Fig. 5.

A. Intrachannel hopping

In the first mechanism, illustrated in Fig. 5(a), alkalis are mainly coordinated to NBO's corresponding to the MRN illustrated in Fig. 1(a). There are no aluminums present so $R=0$. This type of hopping will be the dominant mechanism in silicate glasses where the modifying oxide is sufficiently concentrated for percolation channels to be established,[20] which also happens to be the level of modifier commonly employed in commercial glasses, for example. Accordingly, we refer to this mechanism as *intrachannel hopping*. Because of the association between alkalis and NBO's, intrachannel hopping must involve the local redistribution of NBO and BO configurations

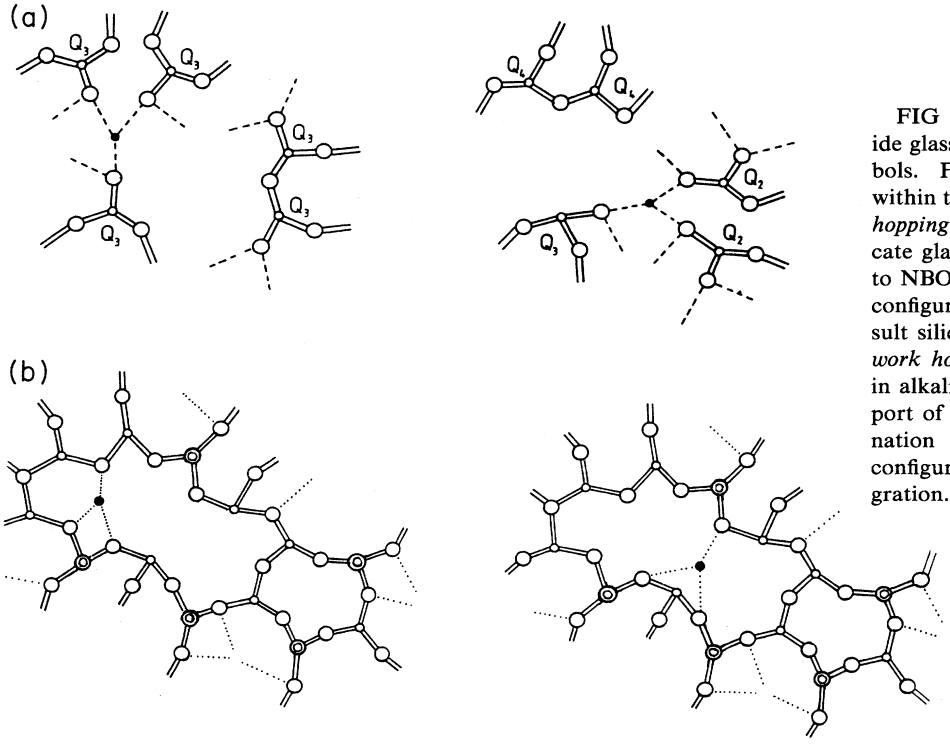

FIG 5. Hopping schemes for alkalis in oxide glasses. Refer to Fig. 1 for the key to symbols. For clarity only one alkali is shown within the alkali-rich clusters. (a) *Intrachannel hopping* anticipated for alkali transport in silicate glasses (Ref. 20). Coordination of alkalis to NBO's necessitates the switching of oxygen configurations to facilitate a hop and as a result silicons disproportionate locally. (b) *Network hopping* appropriate for alkali transport in alkali aluminosilicate glasses and the transport of impurity alkalis in silica. The coordination of alkalis to BO's means minimum configurational change is involved in alkali migration.

and these conformational changes in the network component will result in a contribution to the diffusion enthalpy additional to the electrostatic energy for alkali hopping.

Compared to silica where all silicons are coordinated to four BO's, the presence of NBO's in silicate glasses creates new silicon configurations Q_n, where n refers to the number of nearest-neighbor BO's. Some disproportionation of Q_n's into the Q_{n-1}'s and Q_{n+1}'s occurs in the melt which is subsequently frozen into the glass, i.e.,

$$2Q_n \rightleftharpoons Q_{n+1}+Q_{n-1} . \quad (2)$$

The fractions of the different Q_n's present in a glass are readily obtained using ^{29}Si MASNMR and also Raman spectroscopies.[26] The activation energy $\Delta E_{R=0}$ of the rate constant promoting Eq. (2) at T_g is given by

$$2\Delta E_{R=0} = -kT_g \ln\{(N_{n+1}N_{n-1})/N_n^2\} , \quad (3)$$

where N_{n-1}, N_n, and N_{n+1} are the concentrations of Q_{n-1}, Q_n, and Q_{n+1} configurations frozen into the glass at T_g. It has been shown how $\Delta E_{R=0}$ increases with the weight of the alkali, but remains approximately composition independent for a given alkali.[26] For sodium silicate glasses this is 0.16 and 0.19 eV for potassium silicate glasses, values which we will employ later in calculating enthalpies for alkali diffusion.

While the extent of alkali movement in a glass at T_g is considerable, at lower temperatures we assume that the same processes will persist, but on a less frequent basis. The local disproportionation of Q_n's is therefore an integral part of the intrachannel hopping model proposed for silicate glasses[20] and is illustrated for an alkali disilicate in Fig. 5(a). Mechanistically adjacent oxygens are shown switching locally from NBO to BO configurations and vice versa to accommodate the transfer of the alkali. Recent molecular dynamics studies have confirmed the occurrence of this mechanism in simulated lithium silicate glass structures.[27] We should emphasize, though, that, as there is no net diffusion of oxygen in MD structures or more particularly in oxide glasses, the response of the network to alkali migration will necessarily amount to a "ratchet" mechanism, with oxygens moving backwards and forwards in NBO and BO arrangements and the accompanying silicons alternating between $Q_{n\pm1}$ configurations.

In a MRN representing a silicate glass, then, we propose that the total activation energy for the transfer of a single alkali, E_a, will be made up of the Coulomb term described in the previous section, together with a network conformational term, which we equate with ΔE_R, i.e.,

$$E_a = e^2/4\pi\varepsilon_0\varepsilon_{hf}[1/R_{M\text{-}O} - 1/R_{M\text{-}M}] + \Delta E_R . \quad (4)$$

Taking experimental values for $\Delta E_{R=0}$ determined from Eq. (3), together with $R_{M\text{-}O}$ and $R_{M\text{-}M}$ from XAFS leads to values of E_a for sodium and potassium disilicate glasses of 0.33 and 0.34 eV, respectively, values that are approximately half those of the diffusion enthalpy W reported for the transport of sodium and potassium in these glasses.[24] We stress that Eq. (4) does not include many-body effects ensuing from the other alkalis present, but that E_a is the primitive or microscopic activation enthalpy for the hopping of an isolated alkali.

B. Network hopping

Returning to Fig. 5, alkali hopping through a random network containing no NBO's is shown schematically in Fig. 5(b). We refer to this mechanism as *network hopping*. The alkali is presumed to be bonded only to BO's. This type of hopping is predicted to be the main transport mechanism for the alkalis in CCRN's as illustrated in Fig. 1(b). For the case of an $R=1$ glass, there should be little conformational change in the network accompanying hopping, certainly for the lighter alkalis, in which case we can assume that

$$\Delta E_{R=1} \approx 0 .$$

At intermediate compositions ($0<R<1$) we propose that a mixture of intranetwork and network hopping will prevail, for which the conformational energy ΔE_R will be finite, but less than the value given by Eq. (3). To a first approximation for aluminosilicate glasses where $0<R<1$, we can write

$$\Delta E_R \approx (1-R)\Delta E_{R=0} . \quad (5)$$

From Eqs. (4) and (5), then, we expect the activation enthalpy for ionic diffusion in alkali aluminosilicates to fall with increasing alumina (increasing R), which is indeed observed.[24] However, again we find that calculated values of E_a are approximately equal to half the measured diffusion enthalpy W.

Network hopping is also expected to be the principal hopping mechanism for isolated alkalis present at dilute loadings in silica.[20] In this case the alkali and NBO essentially constitute a defect pair, but there is no reason to suppose that these components will be spatially intimate. At low concentrations an alkali is expected to bond to BO's and to hop to similar sites within what is virtually a CRN in an analogous fashion to alkali diffusion in a CCRN [Fig. 5(b)]. In the case of dilute loadings of alkali in silica, though, there will be no neighboring alkalis present on average and, as we shall discuss, no cooperative effects in the ensuing ionic diffusion. Moreover, hopping distances $R_{M\text{-}M}$ are likely to be larger than within microsegregated regions in silicate or aluminosilicate glasses, in which case the activation enthalpy of alkali diffusion should approach E_b [Eq. (1)]. As we have already demonstrated, values calculated for E_b for sodium and potassium from the local structure are almost identical to the measured diffusion enthalpies for impurity alkali transport.

VI. COOPERATIVE EFFECTS

The cooperative action of alkalis in oxide glasses is manifest in the sublinear frequency dependence of electrical conductivity $\sigma(\omega)$ and, perhaps more obviously, in the behavior of the electric modulus M^* (the reciprocal of the complex dielectric constant ε^*). In particular, the

imaginary part M'' exhibits a pronounced loss peak at some temperature, usually at acoustic frequencies when impedance bridges are used for measurement. The loss peak has a characteristic asymmetric shape that is skewed to higher frequencies. The shape of M'' and of the accompanying M' is well reproduced by incorporating a relaxation function $\phi(t)$ involving a stretched exponential,[28] i.e.,

$$M^*(\omega)=M_\infty\left\{1-\int_0^\infty \exp(-i\omega t)(-d\phi/dt)dt\right\},$$

$$\phi(t)=\exp[-(t/\tau^*)^\beta],$$

where τ^* is the effective relaxation time and β is the Kohlrausch exponent. The loss peak frequency identified in M'' increases with temperature, sharing the same activation energy W as the dc electrical conductivity and signifying a common origin for both ac and dc ionic diffusion processes.[29] It has been argued, however, that Kohlrausch-type relaxation implies anomalous diffusion,[30] in which case the equality of the two activation energies may be a coincidence. On the other hand, Moynihan, Boesch, and Laberge[25,28] have demonstrated that the ac conductivity σ_{ac} calculated from the Kohlrausch law $\exp[-(t/\tau^*)^\beta]$ in the electric modulus formalism has the sublinear $A\omega^{1-\beta}$ frequency dependence characteristic of oxide glasses. Furthermore, this crosses over at $\omega=1/\tau^*$ to assume a finite dc conductivity value. The dc conductivity σ_{dc} can be calculated from Maxwell's equations in terms of the parameters used in the stretched exponential representation of the electric modulus as

$$\sigma_{dc}=\varepsilon_0\beta/[M_{hf}\Gamma(1/\beta)\tau^*],$$

where Γ is the gamma function. M_{hf} is the reciprocal of the dielectric constant at frequencies higher than the conductivity relaxation, i.e., $M_{hf}=1/\varepsilon_{hf}$. The value of σ_{dc} calculated by this expression is found to be almost the same as experiment (see reviews by Angell[31,32]), reaffirming the common basis of ac and dc electrical conductivity processes.

According to many workers' point of view,[31–37] the Kohlrausch exponent β reflects the degree or cooperativity or coupling between the mobile ions in the glass. β has been cataloged for a wide range of oxide glass compositions and typical values lie between 0.5 and 1. Returning to Eqs. (1) and (4), we have already noted how the Coulomb contribution to E_a will decrease with the increase in ε_{hf} associated with addition of modifier to the glass [Fig. 4(a)]. At the same time [see Eq. (4)], the Coulomb contribution to E_a will also fall with the decreasing hopping distances $R_{M\text{-}M}$ associated with microsegregation. Increase in the alkali concentration x will increase the Coulomb interactions and the cooperativity between ions and will be manifest by decreases in β. β analyzed from the electrical conductivity relaxation of $[Na_2O]_x[SiO_2]_{1-x}$ glasses is plotted as a function of x in Fig. 4(b). This reciprocal relationship[20] reflects the increased coupling between the motion of individual alkalis expected in oxide glasses as microsegregated intermediate range order is established. Note how β levels off to values of around 0.5 for alkali concentrations well below the percolation threshold of 0.16, indicating that microsegregation is established at comparatively low alkali loadings, as MD simulations have predicted.[15,16]

Cooperative effects introduce an energy penalty for ionic transport so that, except at the highest frequencies, the macroscopic enthalpy measured in electrical conductivity experiments W will always be greater than the microscopic barrier, E_a. In particular Ngai and Martin[22,33,34] have proposed that W and E_a are related by the expression

$$W=E_a/\beta . \tag{6}$$

For a review, see Ref. 38. Justification for Eq. (6) comes from the coupling model.[39–41] Equation (6) is consistent with many known facts, including the fall in W generally observed for alkali diffusion in glasses with increasing frequency. This is attributed to progressively decreased coupling, with values of β approaching unity and Debye-like relaxation being established at the highest frequencies. In particular, at microwave frequencies, the time constant of nuclear spin relaxation (NSR), which is believed to correlate with ionic motion, is thermally activated with an enthalpy value close to $W_{dc}\beta$, the product of the electrical conductivity enthalpy and the Kohlrausch exponent measured *at low frequencies.*[22,33,34,38,42] From Eq. (6), $W_{dc}\beta$ equals E_a, the microscopic barrier for alkali hopping.

VII. STRUCTURE, COMPOSITION, AND IONIC TRANSPORT IN SINGLE-ALKALI GLASSES

Taking the expressions for E_a for the intrachannel and network hopping mechanisms described above [Eqs. (1), (4), and (5)], parametrized with the structural parameters obtained from alkali XAFS ($R_{M\text{-}O}$ and $R_{M\text{-}M}$) and ^{29}Si NMR ($\Delta E_{R=0}$) together with the high-frequency dielectric constant ε_{hf} and the Kohlrausch exponent β, obtained from electrical conductivity relaxation, we can calculate W from Eq. (6). These values can then be compared directly with the diffusion enthalpies measured by radio tracer diffusion methods[24] and from dc electrical conductivity experiments.[22]

A. Diffusion enthalpies in binary silicates

Starting with the E_a values calculated earlier for intrachannel hopping from the local structure of sodium and potassium in disilicate glasses and the measured β values, Eq. (6) yields macroscopic diffusion enthalpies W of 0.67 and 0.69 eV, respectively, values agreeing with those measured directly[24] to within experimental error. We have already demonstrated how for the network hopping mechanism the alkali binding energies E_b of sodium and potassium given by Eq. (1) closely agree with the measured diffusion enthalpies for dilute concentrations of alkali. As the alkali concentration x increases from impurity loadings upward, we can calculate W separately for intrachannel hopping and for network hopping using the

changing values of β and ε_{hf} given in Figs. 4(a) and 4(b). This is done for $(Na_2O)_x(SiO_2)_{1-x}$ glasses and $(K_2O)_x(SiO_2)_{1-x}$ glasses in Figs. 6(a) and 6(b), respectively. In these comparisons the various elements making up Eqs. (1) and (4) (E_b, E_a, and $\Delta E_{R=0}$) are all indicated.[43] The local structure parameters employed are listed in the figure caption.

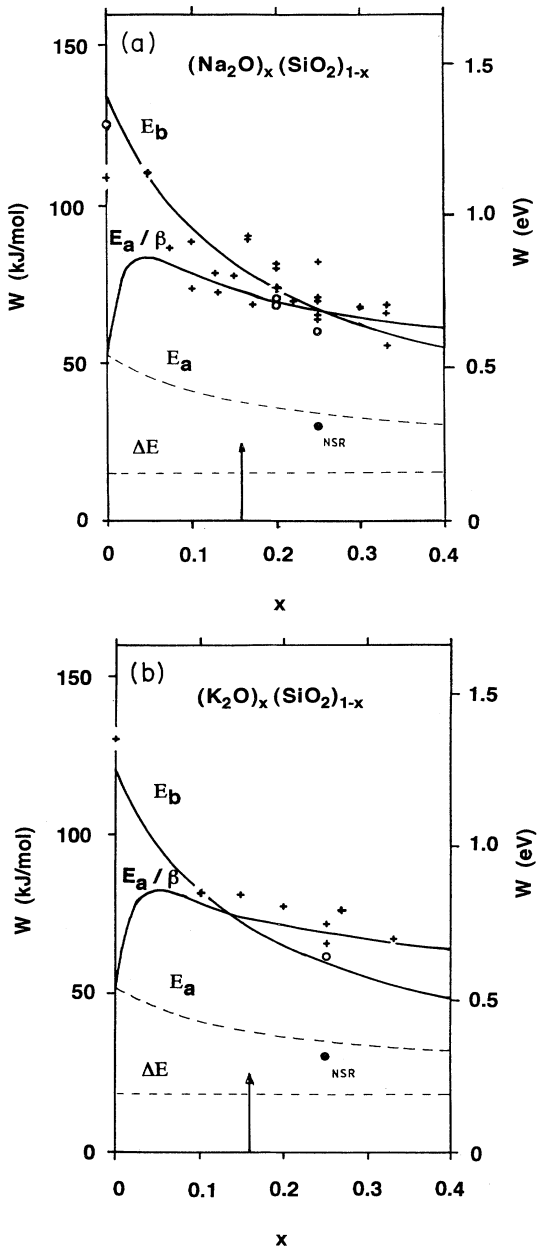

FIG. 6. Diffusion activation energies for sodium and potassium in alkali silicate glasses. Local structure predictions are shown by the solid and dashed curves and directly measured alkali diffusion values by crosses (Ref. 24). Electrical conductivity values are given by open circles and NSR values by solid circles (Ref. 22). The vertical arrow marks the percolation threshold below which network hopping will dominate and above which intrachannel hopping will prevail. (a) For $[Na_2O]_x[SiO_2]_{1-x}$ glasses $R_{M\text{-}O}=2.3$ Å and $R_{M\text{-}M}=3.2$ Å (Ref. 4), $\Delta E=0.16$ eV (Ref. 26), while ε_{hf} and β are taken from Fig. 4. (b) For $[K_2O]_x[SiO_2]_{1-x}$ glasses $R_{M\text{-}O}=2.6$ Å and $R_{M\text{-}M}=3.6$ Å (Ref. 4), $\Delta E=0.19$ eV (Ref. 26), while ε_{hf} and β are again taken from Fig. 4.

It is clear from Fig. 6 that as x is raised, the alkali binding energy E_b falls monotonically as a result of the gradual rise in ε_{hf} values [Eq. (1)], whereas the interchannel enthalpy E_a/β increases abruptly with the initial sharp fall in β [Eq. (6)], eventually exceeding E_b values for higher alkali concentrations. At first glance it appears that E_b offers a reasonable prediction of the fall in W with x for both types of alkali, particularly at low concentrations. If this were the case throughout the composition range, however, it would mean that alkalis always diffuse by the same noninteractive mechanism, with hopping distances large in comparison with oxygen nearest-neighbor distances whatever the alkali-alkali separation. This contradicts the strong evidence for alkali clustering in oxide glasses, the cooperative character of electrical conductivity relaxation in these materials, as well as the dramatic properties of the mixed alkali effect (yet to be discussed), all of which point to interactions between alkalis in oxide glasses. These will dominate once ionic conducting channels are established. The arrows in Fig. 6 mark the percolation thresholds ($x=0.16$) for alkali channels in the two binary glass systems, below which experiment clearly follows the calculated E_b values, while at higher concentrations E_a/β values offer the best all-round agreement. It is important to stress that the E_a/β predictions for intrachannel hopping contain no fitting parameters, but are based on published data. As such, they establish quantitative consistency across the experimental manifold of alkali diffusion, impedance-frequency, XAFS, and MASNMR measurements for these well-studied oxide glasses.

Accordingly, we interpret the characteristic fall in diffusion and dc electrical conductivity enthalpies with increasing alkali content evident in Fig. 3 as being due to a switch from ionic diffusion dominated at first by the hopping of isolated alkalis in the glass network to cooperative hopping through alkali-rich channels, once these have been established. This change matches the development of microstructure resulting from the clustering of alkalis as well as the development of non-Debye-like properties in the ac electrical conductivity. Because the calculated values of E_b and E_a/β are of similar size in the vicinity of the percolation threshold for both sodium and potassium, an abrupt change in activation energy (and hence in diffusivity or in electrical conductivity) is not envisaged for either alkali. Instead, both network and intrachannel hopping are expected to compete up to the establishment of continuous channels. In this heterogeneous regime, intrachannel hopping will always offer the lower-energy barrier to single-particle interchannel hopping, but the macroscopic diffusion enthalpy will be governed by the most difficult hops and these will be encountered in transport of alkalis between channels via the network. At higher concentrations of alkali, when percolation pathways are available, alternative hopping via the network will not in general be required.

At the highest frequencies the coupling model[39–41] predicts that $W \Longrightarrow E_a$. Although NSR results for oxide

glasses are scant to date,[42,44] the nuclear resonance time constant activation energies currently available for sodium and for potassium fall convincingly on the microscopic barrier curve of E_a versus x calculated from Eq. (4) and included in Fig. 6. This bears out the point made earlier that, as the frequency of the applied electric field progressively increases, the motion of a given alkali eventually no longer couples to the motion of other ions in its vicinity and the diffusion enthalpy falls to a minimum.

B. Diffusivity and dc electrical conductivity

When the alkali concentration x is altered in an oxide glass, those differences in hopping distance $R_{M\text{-}M}$ implicit in the two different mechanisms proposed, viz., cooperative intrachannel hopping compared to isolated alkali network hopping, should be manifest. In particular, they should be revealed in the alkali diffusion frequency factor D_0, where the ionic diffusivity D at a particular temperature T is given by Fick's law,

$$D=D_0\exp(-W/kT) . \tag{7a}$$

For classical hopping the diffusion frequency factor is given by

$$D_0=R_{M\text{-}M}^2\nu_0/6 , \tag{7b}$$

where ν_0 is the hopping attempt frequency. Taking the case of silicate glasses for which $x>0.16$ first, ν_0 can be associated with the alkali vibrational band in far-IR absorption.[20] This is 230 cm^{-1} (7×10^{12} s^{-1}) and 170 cm^{-1} (5×10^{12} s^{-1}) for sodium and potassium silicate glasses, respectively.[11] Together with $R_{M\text{-}M}$ values from XAFS, Eq. 7(b) results in values for the diffusion frequency factor D_0 of $\sim10^{-3}$ cm^2 s^{-1} for these glasses. These are in very reasonable agreement with radio tracer experiments where diffusion frequencies of between 10^{-3} and 10^{-2} cm^2 s^{-1} are reported.[24]

By appealing to the Nernst-Einstein relation

$$\sigma_{dc}=Ne^2D/fkT , \tag{8}$$

the same spectroscopy values, together with the alkali concentration N, can be used to predict the electrical conductivity. The Haven ratio f is also included in Eq. (8). Data for the Haven ratio in sodium and potassium silicate glasses are plotted in Fig. 4(c) from Ref. 45. These experiments monitor any discrepancy between the measured diffusivity D and the diffusivity predicted from Eq. (8), $\sigma_{dc}kT/Ne^2$, using dc electrical conductivity measurements. f records the degree of nonrandomness in alkali migration resulting from correlated ionic motion. In an earlier paper[19] we attributed the fall in f with increasing x to developing alkali microsegregation in the glass structures. Despite the scatter in experimental values evident in Fig. 4(c) (which like Fig. 3 is probably related to the tendency for phase separation), f clearly approximately equals $\frac{1}{3}$ for $x>0.16$. For these compositions microsegregation will be fully established and ionic motion in single-alkali glasses is therefore expected to be strongly correlated as it is cooperatively engaged. Note in comparing Figs. 4(b) and 4(c) the qualitative similarity in the dependence on alkali concentration of both f and β.

Using Eqs. (7) and (8) parametrized with the local structure, composition, and IR frequency data, we can therefore calculate the preexponent in the electrical conductivity, $(\sigma_{dc}T)_0$, where

$$\begin{aligned}&\sigma_{dc}T=(\sigma_{dc}T)_0\exp(-W_{dc}/kT) ,\\ &(\sigma_{dc}T)_0=Ne^2R_{M\text{-}M}^2\nu_0/6fk .\end{aligned} \tag{9}$$

For sodium disilicate glass a $(\sigma_{dc}T)_0$ value of 9×10^4 Ω^{-1} cm^{-1} is predicted and for potassium disilicate 8×10^4 Ω^{-1} cm^{-1}. These values are close to the experimental preexponents found for most stable alkali silicate glasses, which typically lie between 5×10^4 and 5×10^5 Ω^{-1} cm^{-1} deg K. Successfully estimating $(\sigma_{dc}T)_0$ from the local structure and alkali concentration (x) underlines the fact that for these compositions ($x>0.16$) a large fraction, if not all, of the alkalis is involved in ionic transport; i.e., oxide glasses behave as strong electrolytes.

As the concentration of alkali, x, falls in binary silicates we have seen from Fig. 3 how the measured hopping activation enthalpy W rises, an increase which we have attributed to the onset of isolated alkali network hopping from considerations of intermediate-range structure. These changes in the measured values of W are generally mirrored by dramatic increases in D_0. For sodium silicate glasses, D_0 recorded in radio tracer experiments rises from disilicate compositions through approximately two orders of magnitude as impurity concentrations of sodium are reached.[24] At these levels of dilution, we envisage that all alkalis are most likely to be completely isolated, in which case the hopping attempt frequency ν_0 should now be dominated, not by the localized phonons associated with Na-O vibrations, but by the itinerant phonons related to the network matrix which have a much higher frequency. For silica the principal stretching modes occur at 1200–1300 cm^{-1}. Such an increase in ν_0 would account for a rise of between 5 and 6 in the alkali diffusion frequency D_0. The remaining contribution to the observed rise in D_0 for sodium transport in silica compared to silicate glasses can be accounted for by an increase in the hopping distance $R_{M\text{-}M}$ from around 3 to around 10 Å.

C. Alkali transport in aluminosilicate glasses

Turning next to alkali transport in aluminosilicate glasses, we have argued earlier that a reduction in the number of NBO's will progressively reduce the conformational energy component ΔE_R of W. As alumina is added to the composition and R increases, the glass structure becomes more polymerized, and we propose that ΔE_R should decrease according to Eq. (5). Diffusion enthalpy data for sodium aluminosilicate glasses taken from Ref. 24 are collated in Fig. 7. This is for the ternary system $[Na_2O]_x[Al_2O_3]_{xR}[SiO_2]_{1-x(1+R)}$ with compositions across the full alumina range of $0<R<1$. Data have been chosen, however, so that variations in the sodium concentration are limited to $0.25<x<0.3$ in order to highlight effects relating to NBO removal and to avoid changes in ε_{hf} that would inevitably result from large

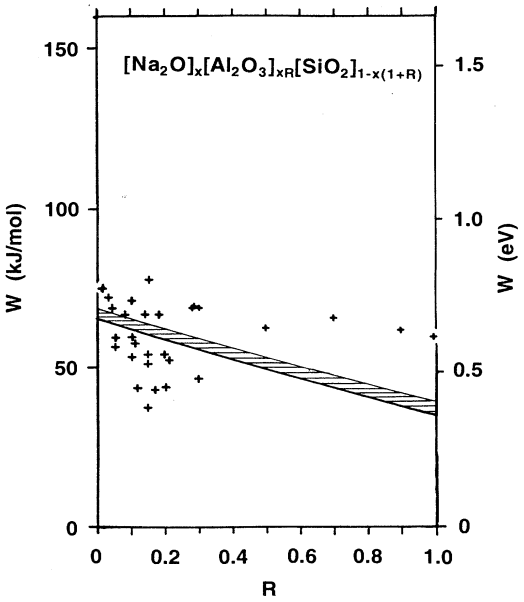

FIG. 7. Diffusion activation energies W for sodium aluminosilicate glasses of general composition $[Na_2O]_x[Al_2O_3]_{xR}[SiO_2]_{1-x(1+R)}$, where $0.25<x<0.33$ and $0<R<1$. W is plotted as a function of alumina content R, the molar ratio Al_2O_3:Na_2O. The hatched bar contains the values of W predicted from Eq. (10) with local structure parameters given in the caption of Fig. 6(a) for the range of x chosen.

differences in alkali content.

Although there is considerable scatter in the enthalpies collected in Fig. 7, it is clear that the activation enthalpy for sodium transport systematically falls as Al_2O_3 replaces SiO_2. We proposed earlier [Eqs. (4) and (5)] that the microscopic enthalpy for intrachannel hopping of a given alkali in an aluminosilicate glass should be given by

$$E_a = e^2/4\pi\varepsilon_0\varepsilon_{hf}[1/R_{M\text{-}O} - 1/R_{M\text{-}M}] + (1-R)\Delta E_{R=0} \, . \tag{10}$$

Taking the values of ε_{hf}, $R_{M\text{-}O}$, $R_{M\text{-}M}$, and ΔE for sodium silicate glasses employed in Fig. 6, values of E_a can be calculated for sodium aluminosilicate glasses as a function of alumina content R.

In order to calculate W using Eq. (6), however, β ideally needs to be measured for the aluminosilicate glass compositions in question. These values are not available; nor are they available to date in general except for particular oxide glass systems, like the sodium silicates illustrated in Fig. 4(b). In the absence of comprehensive Kohlrausch measurements, we make use here and later in this paper of a remarkable empirical relationship between β and W that has been reported by Ngai and Martin across all the oxide glasses so far measured.[22] Indeed, these authors observe that the correlation between electrical relaxation and activation enthalpy is strengthened if W is replaced by $W\beta$. From Eq. (6), $W\beta$ can be equated with E_a, the primitive activation enthalpy for ionic diffusion. This "universal trend" is shown in Fig. 8(a),

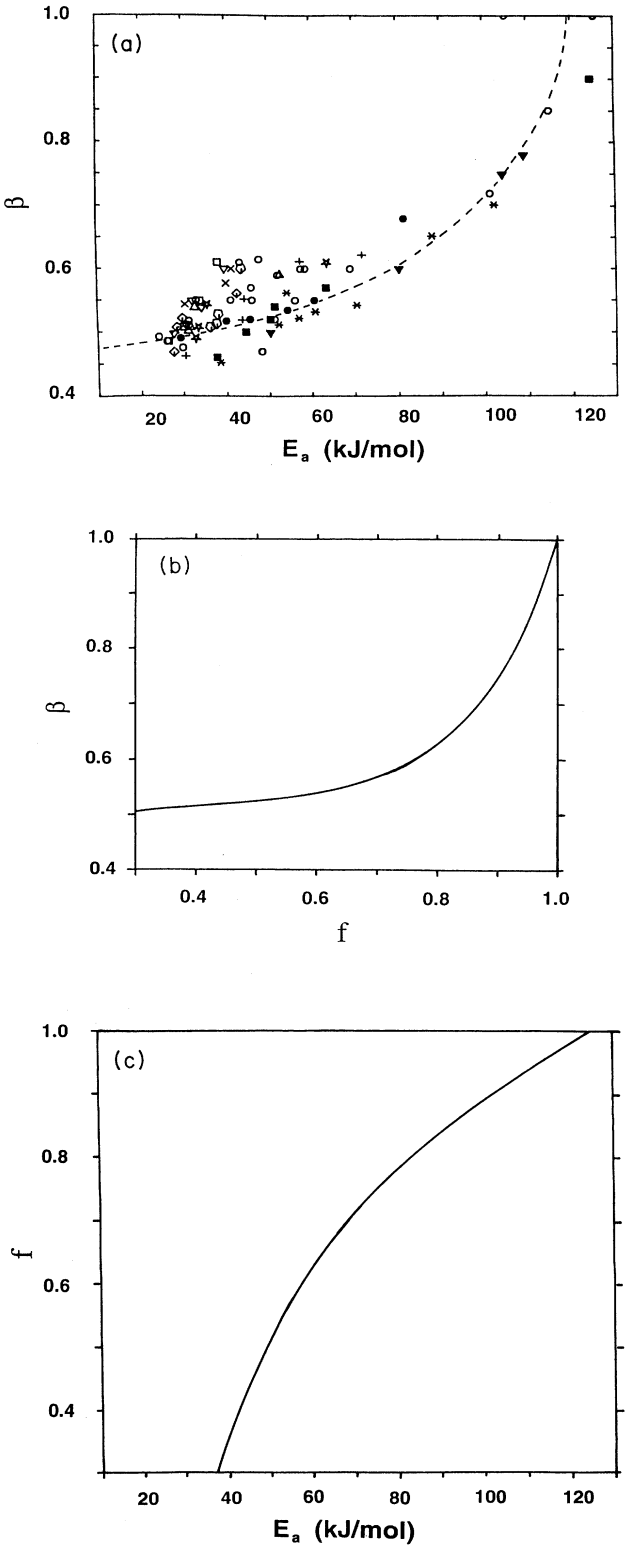

FIG. 8. Empirical correlations between the Kohlrausch exponent β, the Haven ratio f, and the primitive or microscopic activation energy E_a for alkali conduction in oxide glasses. (a) β versus E_a (Ref. 22), (b) β versus f obtained by subsuming Figs. 4(b) and 4(c), and (c) f versus E_a obtained by combining Fig. 8(a) with Fig. 8(b).

which compiles data from concentrated and dilute glasses as well as mixed alkali compositions. The dashed line represents the average relationship between β and E_a and demonstrates how the degree of coupling through cooperative effects $(1-\beta)$ decreases with the increasing activation enthalpy of the mobile alkali. Accordingly, starting with calculated values of E_a for a particular glass system, we can use Fig. 8(a) to obtain the values expected for the Kohlrausch exponent β.

The above procedure has been followed for the aluminosilicate compositions covered in Fig. 7, reading the β values off Fig. 8(a) and combining them with the corresponding E_a's in order to predict the expected macroscopic diffusion enthalpy W using Eq. (6). The cross-hatched region in Fig. 7 contains the predicted values for W within the composition limits of $0.25 < x < 0.33$. The general agreement between these predictions and the absolute values of the measured diffusion enthalpies is good. The slight curvature in the predicted W versus R curves is due to curvature in the "β versus E_a" relationship [Fig. 8(a)]. Nonetheless, the fall in W with increasing R appears to be overestimated as fully compensated compositions are reached (i.e., $R \Longrightarrow 1$). As we saw earlier in Fig. 2, $R_{M\text{-}M}$ can be larger for aluminosilicates than for silicate glasses which would lead to larger values of E_a [Eq. (4)] and hence of W as R approaches 1. Finally, the diffusion frequencies D_0 accompanying the measured activation enthalpies plotted in Fig. 7 typically lie around 10^{-3} cm^2 s^{-1} (Ref. 24) and are consistent with $R_{M\text{-}M}$'s of 3–4 Å and hopping attempt frequencies ν_0 of 10^{12}–10^{13} s^{-1} characteristic of local structure spectroscopy in alkali aluminosilicate glasses.

D. Prerequisites for fast ion conductors

Given the virtual invariance of $(\sigma_{dc}T)_0$ for a given alkali concentration among oxide glasses where $x \geq 0.16$, we can appeal to the expression for the activation energy W given by Eqs. (6) and (10) to emphasize the requirements for fast ion conductors. Clearly, the removal or reduction in the number of NBO's will reduce or eliminate ΔE_R as will the choice of a small or deformable cation. The inclusion of heavy elements in the glass composition will serve to increase ε_{hf}, which will decrease the Coulomb contribution to E_a. Likewise, a decrease in the hopping distance, which often accompanies cations with a low oxygen coordination number, will also help to reduce the electrostatic barrier. Of course, β will also decrease with lower values of E_a, but Fig. 8(a) shows that this dependence becomes progressively weaker as the magnitude of E_a falls. We can recognize many of the ingredients required to lower E_a, and hence W, operating in glasses like $Ag_5I_4BO_3$ and $(AgI)_{0.85}(Ag_4P_2O_5)_{0.15}$.

E. Relationship between the Kohlrausch exponent and the Haven ratio

Finally, returning to Fig. 4, we address the considerable similarity between the compositional dependences of the Kohlrausch exponent β and the Haven ratio f: Both fall monotonically with increasing alkali content x. At the same time, where β is leveling off for values of x starting around 0.05, for f this does not occur until x reaches 0.10–0.15. Nevertheless, both β and f exhibit reciprocal dependences with respect to x, which we attribute to the onset of microsegregation of the alkalis and to the establishment of percolation pathways.[19] We have already argued in this paper how these changes in intermediate-range order in the glass structure explain the decrease in β from 1, when an alkali is present at impurity concentrations and migration occurs in isolation, to values of around 0.5 as x increases and cooperative effects set in due to alkali clustering. In a similar fashion, at dilute alkali loadings, the diffusion will be truly random and D will equate to $\sigma_{dc}kT/Ne^2$, leading to Haven ratios of unity [Eq. (8)]. At higher concentrations, however, the microsegregation of alkalis will mean the involvement of other neighboring alkalis in the diffusion of a given alkali. Migration will cease to be random, which will reduce D, but not $\sigma_{dc}kT/Ne^2$. Accordingly, values of f less than 1 are expected as x increases.

There is an obvious correlation between β and f evident when Figs. 4(b) and 4(c) are compared. Since both sets of data refer to ionic transport in binary sodium and potassium silicate glasses, by eliminating x we can obtain the relationship between β and f shown in Fig. 8(b). From this dependence there are clearly substantial changes in β where f is close to unity and vice versa in f when $\beta \sim 0.5$. Considering Fig. 8(b) in conjunction with Fig. 8(a) reveals a dependence of the Haven ratio f on E_a, the microscopic activation enthalpy for alkali transport. This is shown in Fig. 8(c), the result of combining results from the two figures. Note that the curvature of f versus E_a is opposite in sense to the curvature of β versus E_a. In particular, f changes most rapidly when diffusion enthalpies are small, whereas β changes least in this regime. The relationship between f and E_a shown in Fig. 8(c) has been derived primarily from transport data for single-alkali binary silicates; we anticipate similar "f versus E_a" dependences for other oxide glasses. Whether these fall on the same "universal curve" as in Fig. 8(c) or whether there are families of "f versus E_a" for different oxide glass systems remains to be established. The two relationships shown in Figs. 8(a) and 8(c) will be used later to distinguish the varying transport dynamics of different alkalis in the same oxide glass system and hence rationalize the mixed-alkali effect.

VIII. MIXED-ALKALI EFFECT

A. Electrical conductivity and diffusion coefficients

When more than one alkali is present in a glass, dynamic properties exhibit huge departures from Vegard's law.[1] The electrical conductivity, for example, is dramatically depressed, reaching a minimum around the 50/50 composition. This is illustrated in Fig. 9(a) where electrical conductivity results for seven alkali glasses in the series $([K_\gamma Na_{1-\gamma}]_2O)_{0.25}(SiO_2)_{0.75}$ are plotted from Ref. 46, where γ is the molar ratio of K/Na. At 50°C, σ is shown falling by approximately four decades, and although the size of this minimum decreases with increasing temperature, it still amounts to two decades at 250°C.

Note too how the shape of the isothermal electrical conductivity is not quite symmetrical, reflecting the fact that at these alkali concentrations $W_{Na} < W_K$ in single-alkali glasses (see experiment and prediction in Figs. 3 and 6, respectively). The fall in σ at a fixed temperature for intermediate values of γ is primarily due to radical changes and differences in the diffusion coefficients of the individual alkalis for mixed-alkali glass compositions. The radio tracer diffusion coefficients for sodium and potassium in $([K_\gamma Na_{1-\gamma}]_2O)_{0.25}(SiO_2)_{0.75}$ glasses[46] complementing the $\sigma(\gamma)$ data in Fig. 9(a) are reproduced in Fig. 9(b). Each coefficient falls progressively with increasing foreign-alkali concentration, reminiscent of the compositional dependence of the electrical conductivity. Indeed, Varshneya has demonstrated how, by adapting the Nernst-Einstein equation [Eq. (8)], the dc electrical conductivity can be calculated as a function of alkali composition from the separate diffusivities measured for individual alkalis, each weighted by γ and $1-\gamma$ for potassium and sodium, respectively.[47]

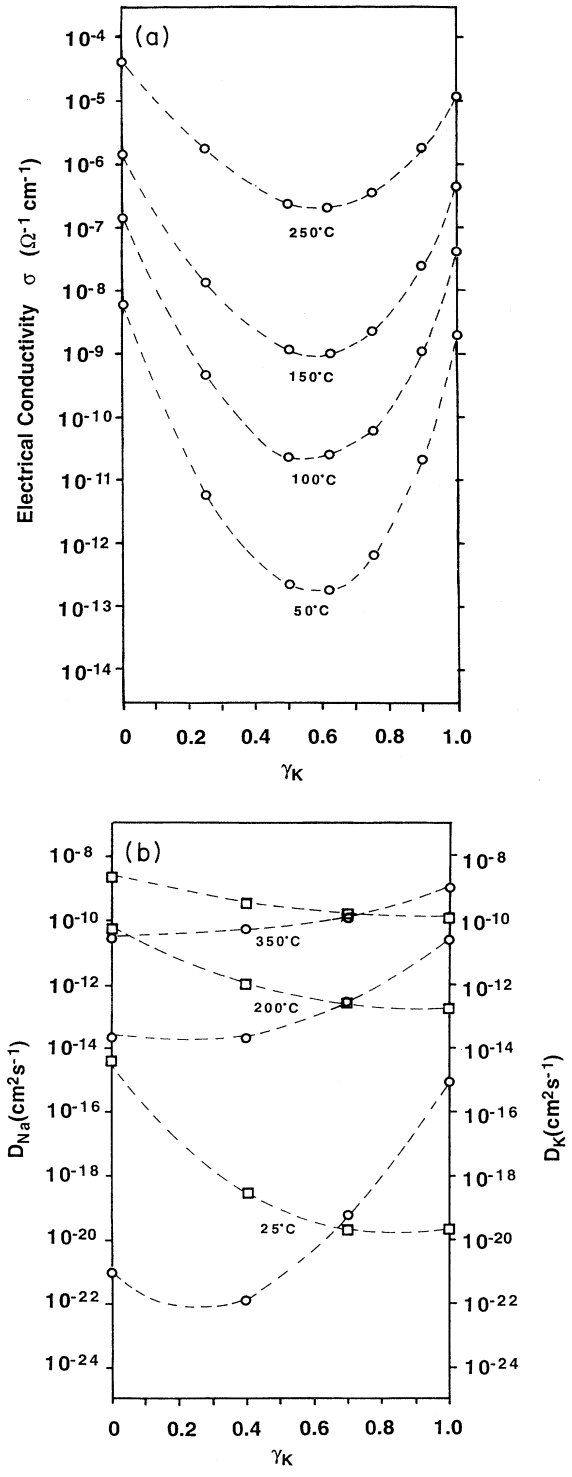

FIG. 9. (a) Electrical conductivities and (b) isothermal diffusion coefficients for sodium (□) and potassium (○) for the mixed-alkali glasses $([K_\gamma Na_{1-\gamma}]_2O)_{0.25}(SiO_2)_{0.75}$ (Ref. 46).

B. Dependence of activation enthalpies on composition

As the preexponent of the electrical conductivity $(\sigma_{dc}T)_0$ for mixed-alkali oxide glasses generally stays within the same bounds for single-alkali glasses quoted in the last section,[17] the mixed-alkali effect must originate primarily from increases in the activation enthalpy W. Electrical conductivity activation energies for three glasses in the $([K_\gamma Na_{1-\gamma}]_2O)_{0.25}(SiO_2)_{0.75}$ series[22] are plotted in Fig. 10(a), where W can be seen to almost double for $\gamma=0.5$ compared to $\gamma=0$ or 1. Further experimental data for sodium-lithium aluminosilicates are included in Fig. 10(b),[48] where the same qualitative behavior is observed, but where the absolute changes are reduced compared to potassium-sodium silicate glasses. Moreover, as we observed for sodium aluminosilicate glasses earlier (Fig. 7), W decreases with alumina content (increasing R) both for lithium aluminosilicates and for mixed-alkali compositions as well. Note too, though, how the mixed-alkali effect is exaggerated by the presence of alumina[48]—the increase in W for mixed ($\gamma_{Li}=0.5$) as opposed to single-alkali glasses ($\gamma_{Li}=0,1$) is greater for $R=1$ than for $R=0.25$.

In trying to understand the variation in W with γ in Figs. 10(a) and 10(b), we believe the changes reported for the diffusion enthalpies of the separate alkalis[24] particularly instructive. The minority alkali exhibits an activation enthalpy approaching that of impurity loadings for the same alkali in silica, while the activation enthalpy of the majority alkali is almost indistinguishable from that in a single-alkali glass; for each alkali, the diffusion enthalpy falls monotonically as its relative concentration increases. Separate values for W_K and W_{Na} for four potassium-sodium glasses of composition $([K_\gamma Na_{1-\gamma}]_2O)_{0.25}(SiO_2)_{0.75}$ (Ref. 49) are plotted in Fig. 10(c). Quite clearly, transport of an alkali at minority loadings is hugely slowed down by the presence of the other alkali, but transport of the same alkali, when this is present as the major constituent, is scarcely affected by impurity loadings of the other. Note in particular, comparing Fig. 10(c) with Fig. 10(a), that at intermediate compositions ($\gamma \approx 0.5$) $W_K \approx W_{Na} \approx W$.

The thermally activated origin of the mixed-alkali effect naturally accounts for the observed reduction in the

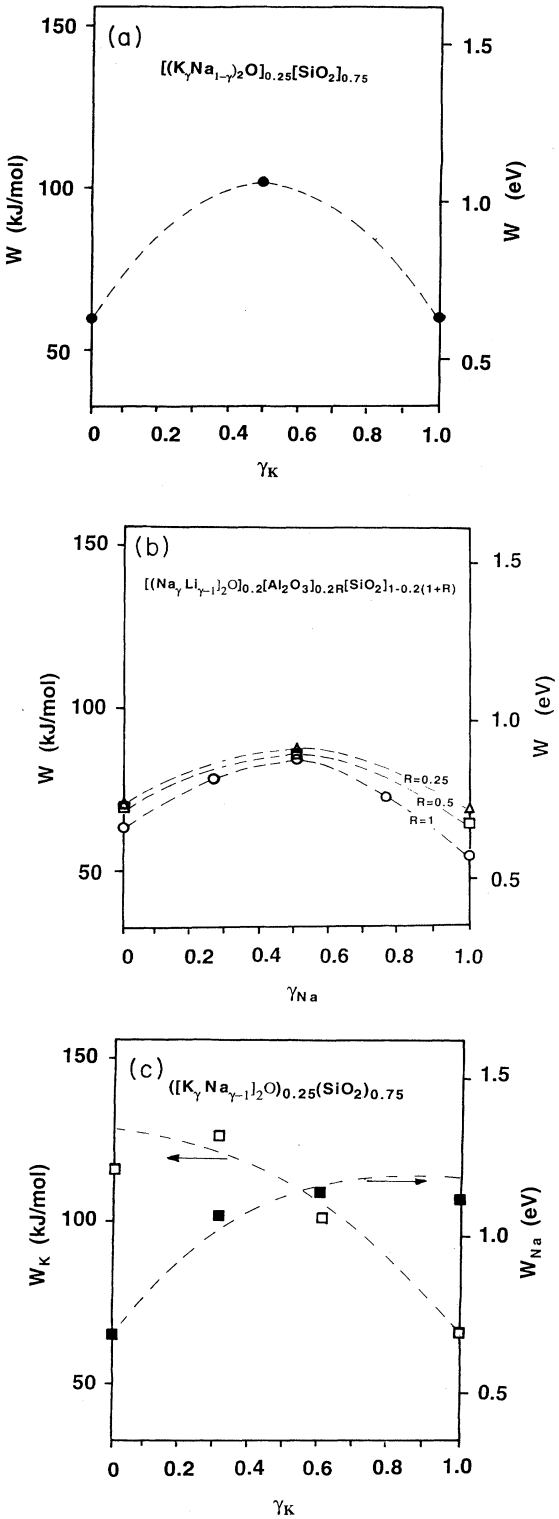

FIG. 10. Experimental dc electrical conductivity activation enthalpies W (a) in mixed-alkali silicate glasses $([K_\gamma Na_{1-\gamma}]_2O)_{0.25}(SiO_2)_{0.75}$ (Ref. 22) and (b) in mixed-alkali aluminosilicate glasses $([Na_\gamma Li_{1-\gamma}]_2O)_{0.2}(Al_2O_3)_{0.2R}(SiO_2)_{1-0.2(1+R)}$ (Ref. 48). Diffusion activation enthalpies W_{Na} and W_K for sodium and potassium in $([K_\gamma Na_{1-\gamma}]_2O)_{0.25}(SiO_2)_{0.75}$ (Ref. 49) glasses.

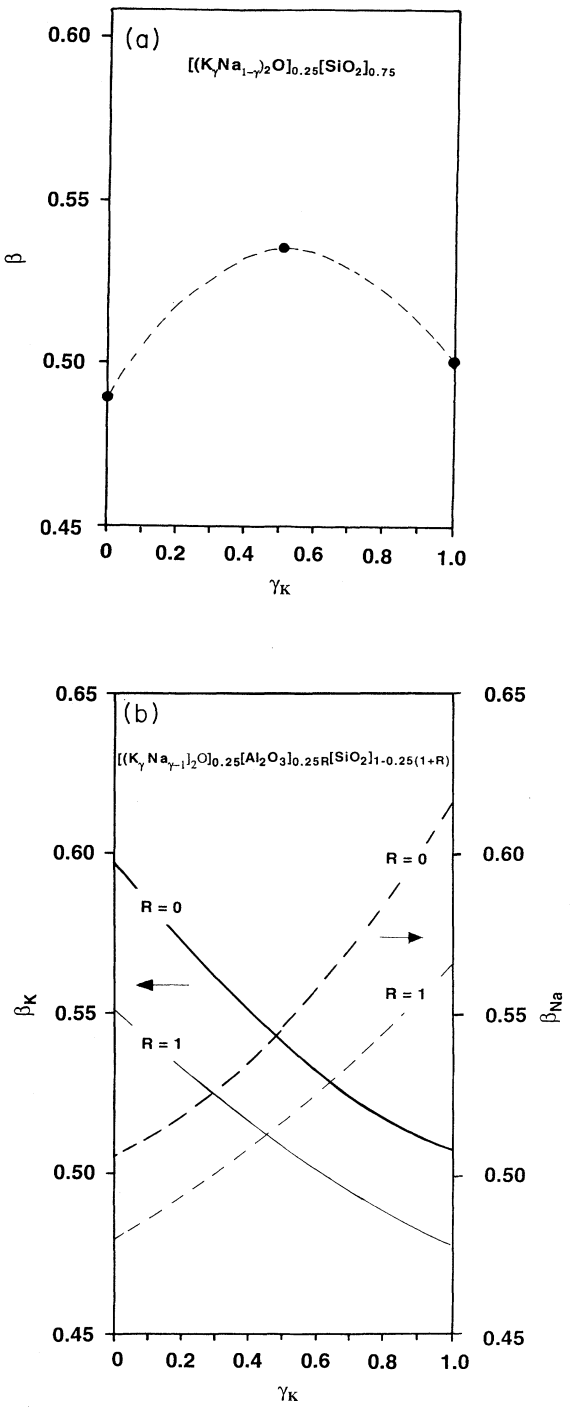

FIG. 11. Measured and predicted Kohlrausch exponents for potassium and sodium silicate glasses. (a) Values of β obtained directly from electrical conductivity measurements (Ref. 22) on $([K_\gamma Na_{1-\gamma}]_2O)_{0.25}(SiO_2)_{0.75}$ glasses. (b) β_K and β_{Na} for $([K_\gamma Na_{1-\gamma}]_2O)_{0.25}(SiO_2)_{0.75}$ glasses obtained from predictions of E_{aK} and E_{aNa} from local structure [Eq. (12) and Fig. 14] in conjunction with the universal β versus E_a curve [Fig. 8(a)]. The complementary values for the equivalent $R=1$ glass $([K_\gamma Na_{1-\gamma}]_2O)_{0.25}(Al_2O_3)_{0.25R}(SiO_2)_{1-0.25(1+R)}$ are also shown. Note how in each case the coupling increases with the concentration of the individual alkali (i.e., β decreases).

size of the effect with increasing temperature [see Fig. 9(a)]. It is also responsible for a corresponding diminution in the effect with increasing frequency. We have already pointed out how W decreases substantially at high frequencies in single-alkali glasses. Recent NSR measurements on $([Na_\gamma Li_{1-\gamma}]_2O)_{1/3}(SiO_2)_{2/3}$ glasses[44] demonstrate that mixed-alkali glasses exhibit similar behavior. In particular, for measurements at 1.5×10^8 Hz, the increase in the diffusion enthalpy of lithium, W_{Li}, for adding sodium is significantly less than the increase in the enthalpy for dc electrical conductivity, W. These differences will automatically lead to shallower diffusion and electrical conductivity isotherms at elevated frequencies, as is generally observed.[1]

C. Kohlrausch exponent and Haven ratio

The increased enthalpies for diffusion and for electrical conductivity found in mixed-alkali oxide glasses are also reflected in the changes reported for the Kohlrausch exponent[22] β and in the Haven ratio f.[50] In both cases these exhibit maxima for a given glass system at $\gamma\approx0.5$. In particular, mixed-alkali compositions reveal a narrowing of the electric modulus peak which is commensurate with a small increase in β of about 10%. Results for $([K_\gamma Na_{1-\gamma}]_2O)_{0.25}(SiO_2)_{0.75}$ glasses are plotted in Fig. 11(a). Alkali diffusion in mixed-alkali glasses is more random than in single-alkali glasses, and this leads to increases in f which can be considerable. Figure 12(a) shows the data for $([Cs_\gamma Na_{1-\gamma}]_2O)_{0.25}(SiO_2)_{0.75}$ glasses where f clearly rises by 3 or 4 times for mixed compared to single-alkali glasses. The changes in β and f evident in Figs. 11(a) and 12(a) are directly attributable to the empirical relationships described earlier between β and E_a [Fig. 8(a)] and between f and E_a [Fig. 8(c)]. When E_a is obtained experimentally from the electrical conductivity enthalpy W using Eq. (6), the maxima in W that characterize the mixed-alkali effect [illustrated in Figs. 10(a) and 10(b)] will naturally lead to maxima in β and f. Moreover, the differences in the curvature of "β and E_a" and compared to "f and E_a," which we have referred to in contrasting Figs. 8(a) and 8(c), explain why the rise in β versus γ [Fig. 11(a)] is smaller than the rise in f versus γ [Fig. 11(b)], β increasing with E_a and therefore with W far more slowly than f does for stable glasses like tetrasilicates and disilicates.

D. Modeling the mixed-alkali effect

There have been several attempts to mimic the phenomenology of the mixed-alkali effect using MD and percolation techniques.[17,18,51,52] MD calculations have revealed the stochastic mixing of alkalis in the microsegregated regions.[17] In addition, the fall in the rms displacements of alkalis with mixing[18] has replicated the observed crossover in self-diffusion coefficients with γ and the overall drop in electrical conductivity isotherms. In their dynamical structure model for ionic transport in oxide glasses, Maass, Bunde, and Ingram have reproduced the same qualitative behavior with percolation simulations,[51] but using a simple cubic lattice partly occupied by mobile

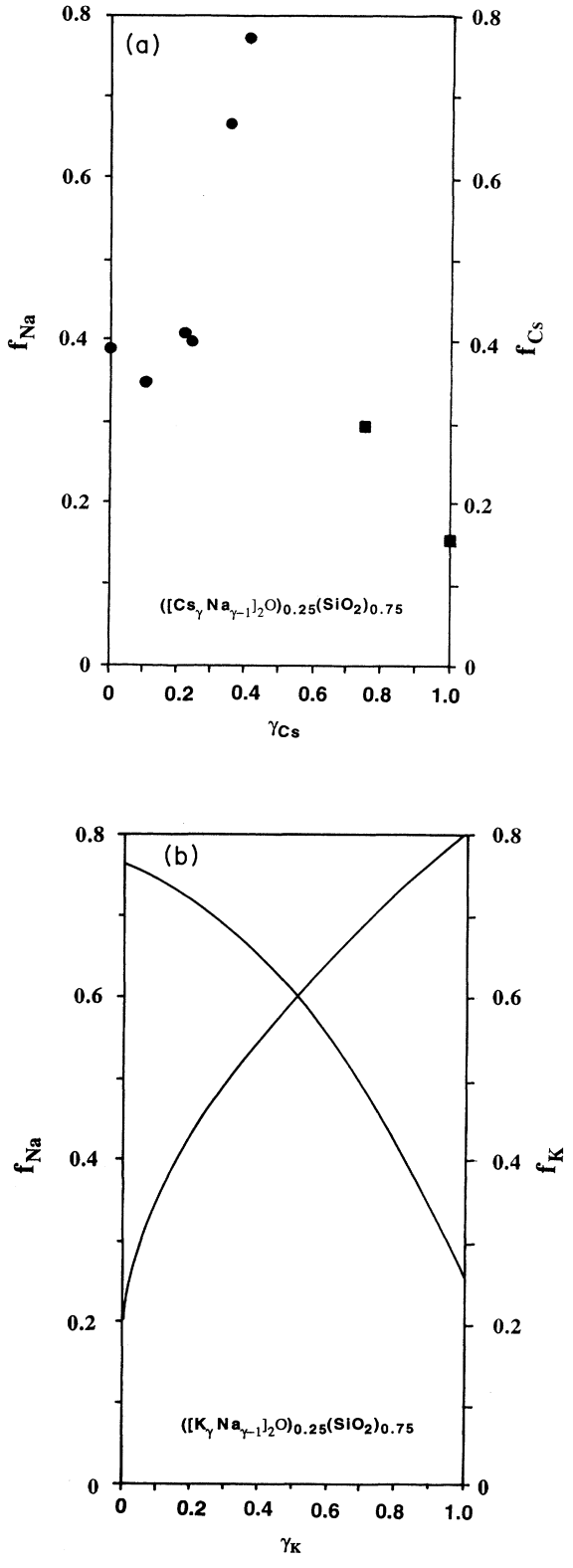

FIG. 12. Measured and predicted Haven ratio values in silicate glasses. (a) f_{Na} (●) and f_{Cs} (■) in $([Cs_\gamma Na_{1-\gamma}]_2O)_{0.25}(SiO_2)_{0.75}$ glasses (Ref. 50). (b) f_{Na} and f_K predicted for $([K_\gamma Na_{1-\gamma}]_2O)_{0.25}(SiO_2)_{0.75}$ glasses, using Figs. 8(c), 14(a), and 14(b).

carriers. Presumably, if this were sunk into the glass network, it would constitute their "connected tissue" of the cluster bypass model.[53] The mixed-alkali effect Maass, Bunde, and Ingram ascribe to mismatches in energy between carriers and vacancies, sites carrying some memory of a previous occupant for a time which is short compared to the hopping time. Finally, Kahnt and Reau[52] have used a bond percolation approach in conjunction with effective-medium-theory results[54] to fit the minima in electrical conductivity isotherms for $([Cs_\gamma Na_{1-\gamma}]_2O)_{0.17}(SiO_2)_{0.83}$ glasses. The diffusion coefficients of caesium and sodium at low concentrations were treated as adjustable parameters along with the bond coordination number or connectivity. In particular, it was necessary for the latter to fall from 6 to almost 2 to fit the isotherms for mixed-alkali glasses, reflecting the substantial reduction in diffusivity of the alkalis for these compositions.

While all of these studies are informative from a heuristic standpoint, they do not, as yet, offer any basis for a quantitative prediction of transport properties, and perhaps more importantly, they fail to untangle atomic structure from the dynamical processes of mobile ions. Following the empirical spirit of this paper, we will make some observations about the separate compositional dependence of the diffusion enthalpies of the alkalis in mixed-alkali glasses illustrated in Fig. 10(c) and then show how the simple ideas that we have put forward in order to predict ionic transport in single-alkali oxide glasses from local structure and electrical relaxation can be extended to account quantitatively for the mixed-alkali effect.

IX. STRUCTURE, COMPOSITION, AND IONIC TRANSPORT IN MIXED-ALKALI GLASSES

A. Alkali-alkali interactions

The variations with composition in the diffusion coefficients and enthalpies for the separate alkalis illustrated in Figs. 9(b) and 10(c) clearly indicate an alkali-alkali interaction. As we have described, the cooperative nature of ionic transport in oxide glasses, which is manifest in the non-Debye character of the electrical conductivity, leads to values of the Kohlrausch exponent β significantly less than unity. Although mixed-alkali glasses exhibit a maximum in β at $\gamma \approx 0.5$ [Fig. 11(a)] which reflects a small *decrease* in coupling, cooperative activity in mixed-alkali transport is still substantial. We have already explained qualitatively how the maximum in β can be correlated with the increase in the dc electrical conductivity enthalpy W illustrated in Fig. 10(a). As W and E_a, the microscopic activation enthalpy, are related through Eq. (6) and β and E_a through the empirical relationship shown in Fig. 8(a), the separate dependences of the diffusion enthalpies of each alkali, W_M, point to *separate β values* for each alkali. Because of the "crossover behavior" of the individual enthalpies of the two alkalis, the corresponding β_M values will behave similarly. In particular, the coupling of each alkali is expected to vary separately with γ, increasing as the proportion of the individual alkali increases.

In the same way independent Haven ratios for different alkalis in a mixed-alkali glass are also expected. From Fig. 8(c), f increases with E_a and therefore for a particular alkali f_M will increase with the diffusion enthalpy W_M. The crossover in diffusion enthalpies with γ illustrated in Fig. 10(a) for W_{Na} and W_K implies, then, similar behavior, not just for β_{Na} and β_K, but also for f_{Na} and f_K. These are the dynamic implications of the complementary changes in the separate diffusion enthalpies of alkalis in glasses of mixed-alkali composition, evident in Fig. 10(c) for sodium and potassium and generally exhibited by other alkali pairs in oxide glasses.[1]

The origin of this bimodal dynamical behavior in mixed-alkali transport is precisely because of the interactions between dissimilar alkalis. Direct structural evidence for alkali-alkali interactions in mixed-alkali glasses has been found from the XAFS of potassium and caesium

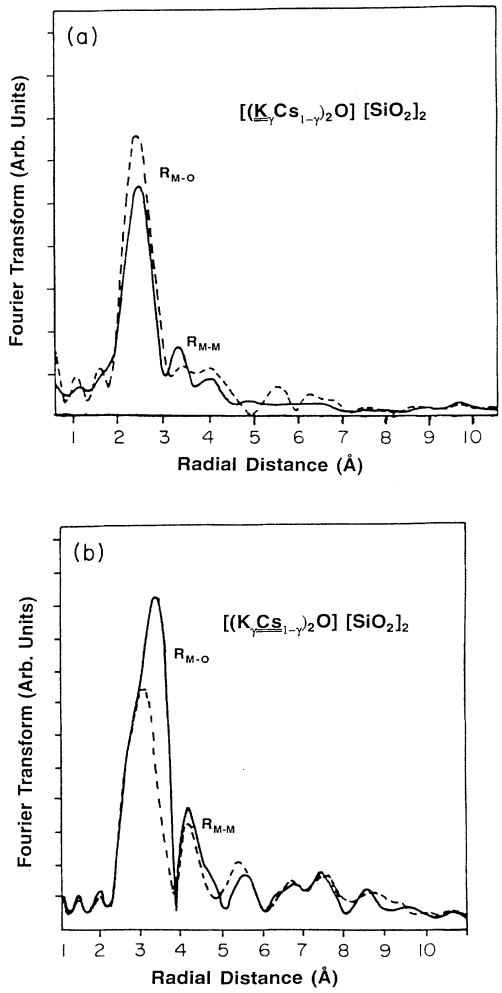

FIG. 13. Partial RDF's for (a) potassium and (b) caesium in single- and mixed-$([K_\gamma Cs_{1-\gamma}]_2O)(SiO_2)_2$ glasses obtained from XAFS spectroscopy (Ref. 23). Single-alkali RDF's ($\gamma = 0, 1$) are shown by solid curves and mixed-alkali RDF's ($\gamma = 0.5$) by dashed curves.

in $[K_\gamma Cs_{\gamma-1}]_2Si_2O_5$ glasses, where the degree of disorder in the nearest-neighbor oxygens surrounding each alkali was found to be affected by the presence of the other alkali.[23] This can be readily seen in Fig. 13 where the partial RDF's for (a) potassium and (b) caesium are reproduced. Solid curves refer to the single-alkali glasses and dashed curves to mixed-alkali glasses. Quite clearly, the nearest-neighbor oxygen peak sharpens for potassium when caesium is present, but shrinks for caesium when potassium is present and curve fitting reveals how the respective Debye-Waller factors are altered, falling for potassium, but increasing for caesium.[23] Clearly, compared to single-alkali glasses, the local ordering of sites occupied by the smaller alkali improves with addition of the heavier alkali to the structure and vice versa. Without intimate mixing the respective partial RDF's of potassium and caesium in these silicate glasses would have remained invariant. Similar conclusions concerning the stochastic distribution of alkalis in borate and silicate glasses have been drawn from analyzing the far-IR bands of single- and mixed-alkali glasses.[11] MD simulations[17] model the same effect. We stress that in all of these studies there is no evidence for the oxygen coordination number of either alkali altering[23] with alkali mixing or for there being any fundamental change in the overall microsegregation of alkalis (irrespective of type) within the glass structure.

B. Predicting separate values of E_a for each alkali from its local structure

Accepting that the microscopic activation enthalpies for transport of alkalis in mixed- and single-alkali glasses can be represented by Eq. (10), we now consider ways in which this might increase when a second alkali is introduced into the environment of the first. Although substantial increases are reported in the low-frequency dielectric constant of alkali silicate glasses when this happens,[55] both single- and mixed-alkali glasses converge on the same value at high frequencies. The values of ε_{hf} given in Fig. 4(a), which increase with alkali concentration x, are representative of single- and mixed-alkali glasses alike. Insofar as $R_{M\text{-}O}$ distances are concerned that define the binding energy of the alkali [Eq. (1)], there is no evidence from XAFS that values are radically affected by the mixing of alkalis.[4,23] Turning next to the conformational energy contribution to E_a, ΔE_R, in Eq. (10), it is interesting to note that the disproportionation of Q_n's measured with ^{29}Si NMR is reported to be not strongly affected by the mixed-alkali proportion γ.[8] According to Eq. (3), the considerable increases in separate E_a's when more than one alkali is present, reflected in the compositional dependences of the W_M's reproduced in Fig. 10(c), cannot be due to increases in the network conformation energy ΔE_R. This draws attention finally to the alkali-hopping distance $R_{M\text{-}M}$. We propose that the presence of more than one alkali causes this to increase, thereby increasing the self-diffusion enthalpy.

Given the stochastic mixing of alkalis in the conducting channels, a plurality of sites must exist for a given γ. Out of these, there will be two extreme cases. When a given alkali is in the majority it will be mainly surrounded by like alkalis and hopping to adjacent sites is the most likely event. The situation is equivalent locally to that described earlier for single-alkali intrachannel hopping [Fig. 5(a)], and so the lower limit of the primitive ac-

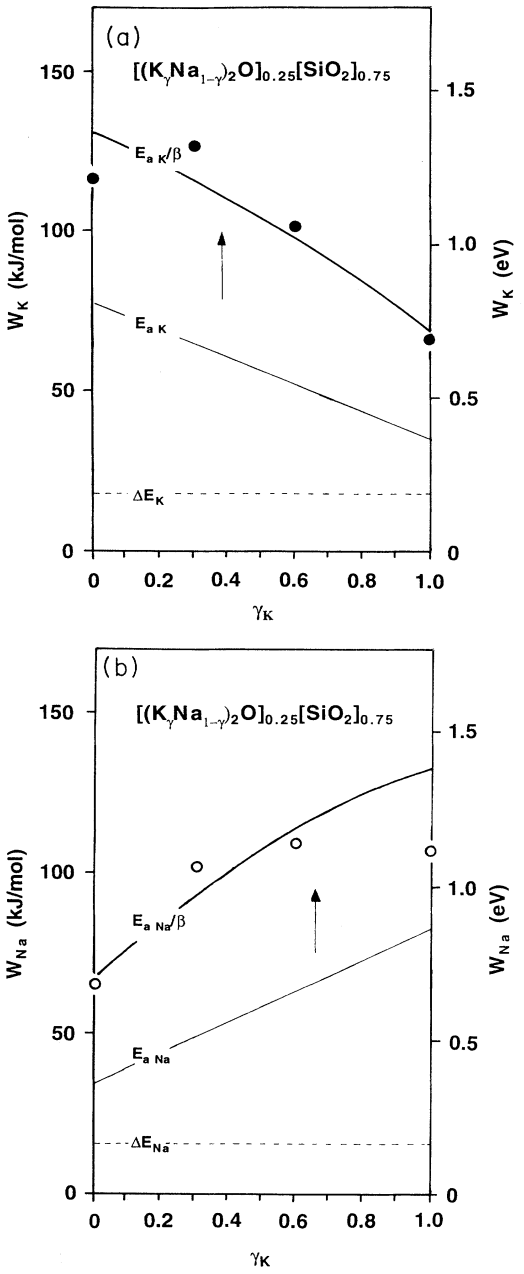

FIG. 14. Self-diffusion enthalpies (a) W_K and (b) W_{Na} predicted for potassium and sodium in the mixed-alkali tetrasilicate glasses $([K_\gamma Na_{1-\gamma}]_2O)_{0.25}(SiO_2)_{0.75}$. Experimental points are from Ref. 49 and plotted in Fig. 3. Solid lines employ Eqs. (12) and (13) and incorporate local structure parameters from the caption of Fig. 6 and β values from Fig. 11(a). The complementary thin solid lines refer to the primitive activation energies E_{ai} and configurational energies ΔE_i for the two alkalis obtained from local structure spectroscopies.

tivation enthalpy for diffusion of one of the alkalis, E_{a1}, will be given by

$$E_{a1} \geq e^2/4\pi\varepsilon_0\varepsilon_{hf}[1/R_{M1\text{-}O} - 1/R_{M1\text{-}M1}] + (1-R)\Delta E_{1R=0} \ . \quad (11a)$$

The second situation will apply to the hopping of minority alkalis, where these are chiefly surrounded by foreign alkalis. In this case the same alkali hops to a distant site where there are fewer steric constraints, but for which the limiting primitive activation enthalpy will now be

$$E_{a1} \leq e^2/4\pi\varepsilon_0\varepsilon_{hf}[1/R_{M1\text{-}O}] + (1-R)\Delta E_{1R=0} \ . \quad (11b)$$

Equivalent expressions to Eqs. (11a) and (11b) for the second alkali can clearly be written down. Between these two extremes there will be a continuum of intermediate possibilities which will be governed by γ_1 and the geometric and packing constraints of the two alkalis. For simplicity we linearly interpolate between Eqs. (11a) and (11b) to obtain the following compositional dependences of the microscopic activation enthalpies for the two alkalis:

$$\begin{aligned} E_{a1} &= e^2/4\pi\varepsilon_0\varepsilon_{hf}[1/R_{M1\text{-}O} - \gamma_1/R_{M1\text{-}M1}] + (1-R)\Delta E_{1R=0} \ , \\ E_{a2} &= e^2/4\pi\varepsilon_0\varepsilon_{hf}[1/R_{M2\text{-}O} - (1-\gamma_1)/R_{M2\text{-}M2}] + (1-R)\Delta E_{2R=0} \ . \end{aligned} \quad (12)$$

Using the structural parameters from Fig. 6, the linear dependences of $E_{a\mathrm{K}}$ and $E_{a\mathrm{Na}}$ on γ_{K} are shown by the thin solid lines in the lower halves of Figs. 14(a) and 14(b), respectively. These are calculated for glasses of composition $([\mathrm{K}_\gamma\mathrm{Na}_{1-\gamma}]_2\mathrm{O})_{0.25}(\mathrm{SiO}_2)_{0.75}$. Confirmation of these predictions from NSR has yet to be made, but we note that $E_{a\mathrm{Li}}$ is reported to increase significantly in $([\mathrm{Na}_\gamma\mathrm{Li}_{1-\gamma}]_2\mathrm{O})_{1/3}(\mathrm{SiO}_2)_{2/3}$ glasses for increasing γ_{Na}.[44] The experimental errors in determining $E_{a\mathrm{Li}}$ from NSR for mixed-alkali compositions, however, are too great in these measurements to confirm the linear dependence proposed here in Eq. (12).

C. Compositional dependences of β and f for each alkali

From arguments that we have already expounded, given a particular mixed-alkali composition γ_i, the motion of each alkali will be differently coupled to the remaining alkalis and hence will be associated with different Kohlrausch exponent values β_i. Following the procedure introduced earlier for determining the values of β expected for aluminosilicate glasses, we can use Eq. (12) to obtain the separate E_{ai}'s for each of the alkalis in a mixed-alkali glass and utilize the "β versus E_a" curve to read off the respective β_i's as a function of composition γ_i. This has been done for sodium and potassium in the tetrasilicate silicate system $([\mathrm{K}_\gamma\mathrm{Na}_{1-\gamma}]_2\mathrm{O})_{0.25}(\mathrm{SiO}_2)_{0.75}$. The changing values of $E_{a\mathrm{K}}$ and $E_{a\mathrm{Na}}$ with γ are given by the thin solid lines in Figs. 14(a) and 14(b), respectively. The corresponding β_i values are plotted with the heavy solid and dashed curves in Fig. 11(b). The crossover value of β is 0.54(2) and the single-alkali end members β_{Na} and β_{K} are 0.50(5) ($\gamma_{\mathrm{K}}=0$) and 0.50(8) ($\gamma_{\mathrm{K}}=1$), respectively. Comparing these figures with the overall β values measured directly from electrical conductivity relaxation[22] [Fig. 11(a)], agreement is better than 1%. Figure 11(b) also contains predictions shown by the dashed curves of β_{Na} and β_{K} for the equivalent $R=1$ aluminosilicate glass system $([\mathrm{K}_\gamma\mathrm{Na}_{1-\gamma}]_2\mathrm{O})_{0.25}(\mathrm{Al}_2\mathrm{O}_3)_{0.25}(\mathrm{SiO}_2)_{0.5}$ where the overall rise in β is smaller. This is commensurate with the decreased curvature of the "β versus E_a" curve [Fig. 8(a)] for the smaller values of E_a.

We can apply this same approach to deduce separate Haven ratios for each alkali in a particular mixed-alkali glass. Taking the E_{Na} and E_{K} values calculated from Eq. (12) for the $([\mathrm{K}_\gamma\mathrm{Na}_{1-\gamma}]_2\mathrm{O})_{0.25}(\mathrm{SiO}_2)_{0.75}$ glass system and reproduced in Fig. 14, we can use the "f versus E_a" relationship given in Fig. 8(c) to read off Haven ratio values for the two alkalis, f_{Na} and f_{K}, as a function of mixed-alkali composition γ. These predictions are shown in Fig. 12(b) and reveal how the Haven ratios of the separate alkalis rise to a maximum of approximately $X3$ compared to the values for single-alkali compositions. No direct comparisons can yet be made with radio tracer experiments for these particular glasses, but the very similar profile of f_{Na} and f_{Cs} reported for $([\mathrm{Cs}_\gamma\mathrm{Na}_{1-\gamma}]_2\mathrm{O})_{0.25}(\mathrm{SiO}_2)_{0.75}$ glasses[50] reproduced in Fig. 12(a) is encouraging.

D. Activation enthalpies for alkali transport

With separate values E_{a1} and E_{a2} for the microscopic diffusion activation enthalpies calculated for the alkalis in a mixed-alkali glass series and with the corresponding β_1 and β_2 figures predicted from Fig. 8(a), the individual macroscopic activation enthalpies W_1 and W_2 can be obtained from local structure by appealing to Eq. (6), viz.,

$$W_1 = E_{a1}/\beta_1 \quad \text{and} \quad W_2 = E_{a2}/\beta_2 \ . \quad (13)$$

The heavy curves shown in the upper half of Figs. 14(a) and 14(b) are the values for W_{K} and W_{Na} obtained from Eqs. (12) and (13) by incorporating the local structure and cooperative dynamics appropriate to potassium and to sodium in the same series of mixed-alkali glasses $([\mathrm{K}_\gamma\mathrm{Na}_{1-\gamma}]_2\mathrm{O})_{0.25}(\mathrm{SiO}_2)_{0.75}$. The agreement with the diffusion activation energies measured directly by radio tracer methods[49] is very satisfactory over most of the composition range, both as far as absolute values are concerned and from the point of view of the sense of curvature of $W_{\mathrm{Na/K}}$ versus γ.

As W is observed to decrease with increasing frequency, so the size of the mixed-alkali effect should likewise decrease. In particular, the crossover dependence of the much smaller microscopic activation enthalpies E_{Na} and E_{K} in Fig. 14 should give rise to a much-diminished mixed-alkali effect at microwave frequencies. This follows the prediction of the coupling model[40,41] that W approaches E_a at the highest frequencies. For the predicted enthalpy values given in Fig. 14, the depth of the corresponding minimum in the room-temperature electrical conductivity isotherm at these high frequencies would be

equivalent to raising the temperature to 300°C under dc conditions.

For the very lowest minority-alkali concentrations, ions in mixed-alkali glasses will no longer have an energy incentive to hop via modifier channels. Comparing Eq. (1) with Eq. (12)

$$E_{a1,2} > E_b \quad \text{as } \gamma_{1,2} \Longrightarrow 0 \ .$$

Accordingly, we anticipate that isolated alkali network hopping will become increasingly likely as the concentration of the minority alkali approaches impurity loadings in mixed-alkali glasses. The compositions at which the predicted microscopic activation enthalpies $E_{a\mathrm{Na/K}}$ exceed the respective alkali-binding energies $E_{b\mathrm{Na/K}}$ are marked by arrows in Figs. 14(a) and 14(b). It is noticeable that these are the $\gamma_{\mathrm{Na/K}}$ values below which Eq. (12) overestimates experiment. The increase in hopping distance for each alkali implicit in Eq. (12) ranges from 3 to 7 Å for single- ($\gamma=0,1$) and mixed-alkali ($\gamma=0.5$) compositions, respectively. As the minority-alkali concentration falls further, larger increases in $R_{M\text{-}M}$ are expected. Evidence for such increases in $R_{M\text{-}M}$ can be found in the measured diffusion frequency values which increase by several decades as the concentration of a particular alkali falls from $\gamma=1$ to impurity loadings ($\gamma\approx 0$) for a fixed x.[49] With the onset of isolated hopping via the network, ν_0 should also increase to network frequencies, as we argued earlier. Referring back to Eq. (7), the dramatic rises reported in D_0 for impurity alkalis in mixed-alkali silicate glasses[24] are attributed to a combination of increases in $R^2_{M\text{-}M}$ and ν_0.

As the *total* alkali concentration x decreases below the percolation threshold, we have argued when considering single-alkali silicates that intrachannel transport will be progressively replaced by the increased occurrence of isolated alkali hopping through the network. As the mixed-alkali effect has been chiefly attributed to intrachannel hopping in the microsegregated regions present in oxide glasses, it is self-evident that the effect will diminish with x, vanishing when the total concentrations of alkali approach impurity loadings, as is indeed observed.[56,57]

E. Predicting alkali diffusivities and dc electrical conductivity

Given the diffusion enthalpies $W_{1,2}$ of the two alkalis calculated from XAFS and MASNMR, the associated $R_{M\text{-}M}$ values also obtained from alkali XAFS and the corresponding ν_0's from far-IR spectroscopy, the separate diffusivities $D_{1,2}$ of each alkali at a particular temperature can be calculated from Eq. (7). Results for sodium and potassium diffusivity predicted for the mixed-alkali series $([K_\gamma Na_{1-\gamma}]_2O)_{0.25}(SiO_2)_{0.75}$ are shown in Fig. 15(a) where they can be compared with experimental values [Fig. 9(b)].[46] The values of D_{Na} and D_{K} for the single-alkali glasses are extremely accurately predicted. The crossover behavior for mixed-alkali compositions is also well reproduced, but there is some divergence of calculated individual diffusion isotherms from experiment with decreasing $\gamma_{\mathrm{Na/K}}$. This is largely due to the Arrhenius character of the diffusion coefficient, and

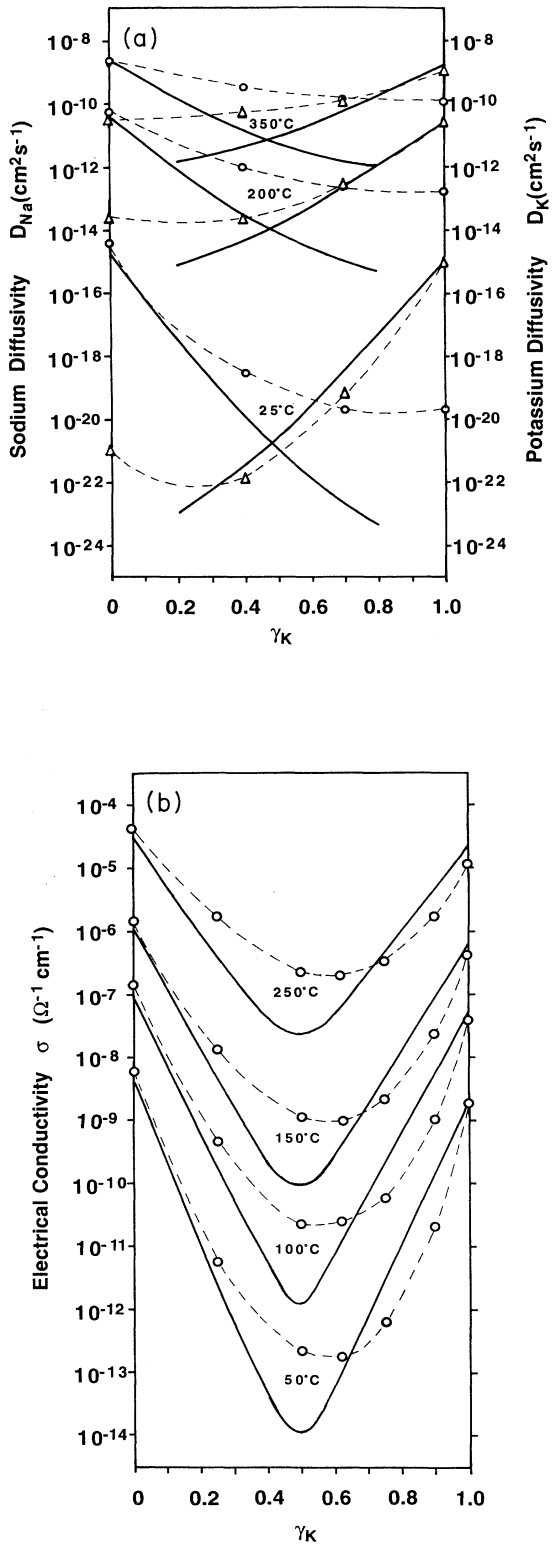

FIG. 15. (a) Isothermal diffusion coefficients and (b) electrical conductivities for the mixed-alkali glasses $([K_\gamma Na_{1-\gamma}]_2O)_{0.25}(SiO_2)_{0.75}$. The experimental points are taken from Fig. 9 (Ref. 46). The solid lines are predicted from local structure employing Eqs. (7), (8), (9), and (10) using the parameters for sodium and potassium given in the caption to Fig. 6.

good agreement can be achieved by small adjustments to the diffusion enthalpies of a few percent, i.e., within the experimental accuracy of the measured values [Fig. 10(c)]. We have refrained, however, from introducing fitting procedures in order to maintain simplicity.

The dc electrical conductivity at a given temperature can be calculated from

$$\sigma_{dc}T=\gamma(\sigma_{dc}T)_{01}\exp(-W_1/kT)$$

$$+(1-\gamma)(\sigma_{dc}T)_{02}\exp(-W_2/kT)\ . \qquad (14)$$

We can take the appropriate $R_{M\text{-}M}$'s from XAFS and ν_0's from IR spectra to calculate the preexponents $(\sigma_{dc}T)_{01,2}$ and use the predicted values of W_1 and W_2 from Fig. 14 to evaluate the electrical conductivity isotherms as a function of γ. Values for $([K_\gamma Na_{1-\gamma}]_2O)_{0.25}(SiO_2)_{0.75}$ glasses are plotted in Fig. 15(b) where they can be compared directly with the measured transport results reported by Moynihan *et al.*[46] The degree of quantitative agreement is again encouraging. The predicted electrical conductivity values for single-alkali glasses agree with experiment to better than a factor of 2 at all temperatures. The minima for mixed-alkali glasses are reproduced, increasing with falling T. On the other hand, the depth of the minima is overestimated by about a decade at worst and the small offset in the position ($\gamma_K=0.5$ rather than 0.6) is lacking. These effects, as noted above in discussing the diffusivities calculated for sodium and potassium, are mainly due to a slight overevaluation of the diffusion enthalpies for mixed-alkali compositions.

Finally, combining Eqs. (9) and (14), the mean dc electrical conductivity activation energy W can be obtained at a particular temperature from

$$\sigma_{dc}T=(\sigma_{dc}T)_0\exp(-W_{dc}/kT)=\gamma(\sigma_{dc}T)_{01}\exp(-W_1/kT)+(1-\gamma)(\sigma_{dc}T)_{02}\exp(-W_2/kT)\ . \qquad (15)$$

Values of W for $([K_\gamma Na_{1-\gamma}]_2O)_{0.25}(SiO_2)_{0.75}$ glasses are given as a function of mixed-alkali composition γ by the upper curve ($R=0$) in Fig. 16, indicating very reasonable agreement with the experimental points for silicate glasses[22] taken from Fig. 10(a).

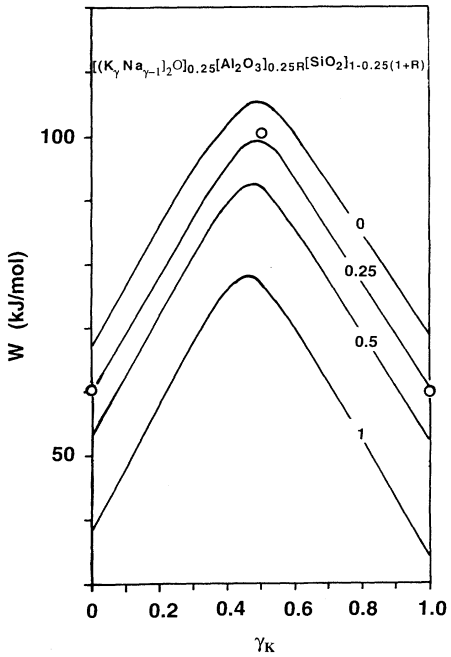

FIG. 16. Predicted dc electrical conductivity activation energies W versus γ for $([K_\gamma Na_{1-\gamma}]_2O)_{0.25}(Al_2O_3)_{0.25R}(SiO_2)_{1-0.25(1+R)}$ glasses obtained from Eq. (15) for $T=400$°C. Points refer to experimental values for $R=0$ silicate glasses taken from Fig. 10(a) (Ref. 22).

F. Enhanced effects in aluminosilicate glasses

Returning to Eq. (10), we can calculate values of $E_{a1,2}$ for the separate alkalis in mixed-alkali aluminosilicate glasses for different Al_2O_3/Na_2O ratios. $\beta_{1,2}$ values can be obtained from the "β versus E_a" curve [Fig. 8(a)] and the corresponding diffusion enthalpies $W_{1,2}$ calculated. The preexponents $(\sigma_{dc}T)_{01,2}$ can be derived as described above and the mean dc electrical conductivity predicted. Values of W calculated for the mixed-alkali aluminosilicates $([K_\gamma Na_{1-\gamma}]_2O)_{0.25}(Al_2O_3)_{0.25R}(SiO_2)_{1-0.25(1+R)}$ are also included in Fig. 16 for R equal to 0.25, 0.5, and 1. The curves are not quite symmetrical, principally because of the larger ΔE_R values for $[K_2O]_{0.25}[SiO_2]_{0.75}$ glasses compared to $[Na_2O]_{0.25}[SiO_2]_{0.75}$ glasses, which we drew attention to earlier in considering single-alkali glasses. In particular, if we assume that the alkali environments in silicate and aluminosilicate glasses are approximately the same and therefore that the Coulomb contributions to the total enthalpy are also similar, then Eq. (10) predicts that the dispersion in W at $\gamma=0$ and 1 should approximate to $\Delta E_i/\beta$. Experimental data for the mixed-alkali glass series $([K_\gamma Na_{1-\gamma}]_2O)_{0.25}(Al_2O_3)_{0.25R}(SiO_2)_{1-0.25(1+R)}$ are not available for a direct comparison to be made with the predictions of W given in Fig. 16, but data for the mixed-alkali glasses $([Na_\gamma Li_{1-\gamma}]_2O)_{0.2}(Al_2O_3)_{0.2R}(SiO_2)_{1-0.2(1+R)}$ have been reported.[48] These results were given earlier in Fig. 10(b). In comparing our predictions with these experiments, we can clearly reproduce the same general behavior in mixed-alkali glasses that we saw earlier for sodium aluminosilicate glasses (Fig. 7), with W decreasing with increasing R, but in this case for all γ. Note too a greater dispersion in W for sodium compared to lithium aluminosilicate glasses, which points to ΔE_{Na} being greater than ΔE_{Li}, in agreement with the results of MASNMR spectroscopy.[26]

Lapp and Shelby[48] pointed out the interesting fact that the addition of alumina to their lithium sodium silicate

glasses resulted in a more accentuated mixed-alkali effect. This can be clearly seen in Fig. 17(a) taken from their results in the different dependences of ΔW on composition. Values are taken from Fig. 10(b) where ΔW is the change in the dc electrical conductivity activation energy with mixed-alkali composition γ. These authors attribute the increased effect at $\gamma=0.5$ for $R=1$ to the removal of NBO's from the glass structure. Included in Fig. 17(b) is the predicted behavior for sodium-potassium aluminosilicate glasses taken from Fig. 16. The same deviation from additivity in W with increasing alumina content or rising R is also reproduced, although the predicted effect is smaller than that reported for the lithium-sodium aluminosilicates.

We can see the reason for the departure from additivity in W in aluminosilicate glasses by referring back to Fig. 11(b), where predictions of β_{Na} and β_K for $R=0$ and 1 mixed-alkali series were compared. The $\beta_{Na/K}$ versus γ characteristics for each of these pairs of curves relate to

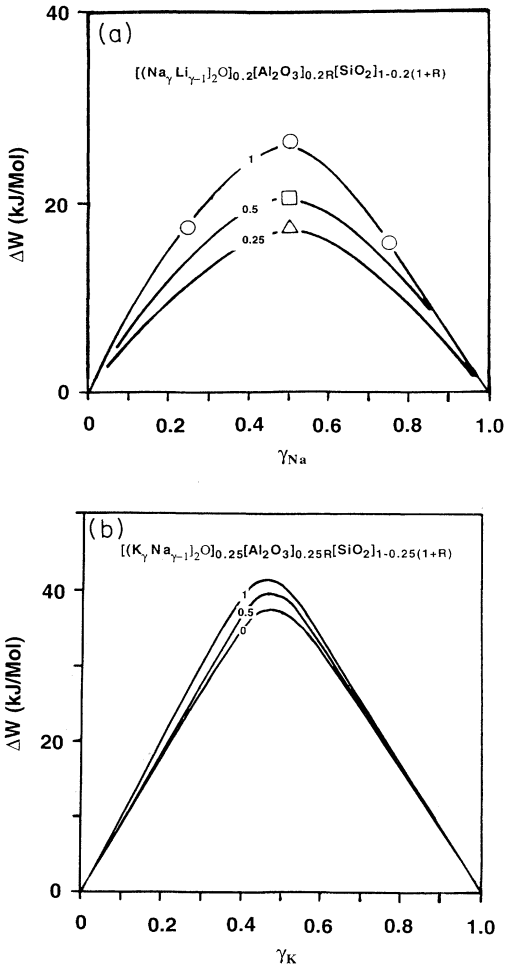

FIG. 17. Increase in the magnitude of the mixed-alkali effect with increasing alumina. The departure from Vegard's law of the dc electrical conductivity activation energy W. (a) Predicted for $([K_\gamma Na_{1-\gamma}]_2O)_{0.25}(Al_2O_3)_{0.25R}(SiO_2)_{0.75(1+R)}$ glasses obtained using the values obtained from local structure in Fig. 16. (b) $([Na_\gamma Li_{1-\gamma}]_2O)_{0.2}(Al_2O_3)_{0.2R}(SiO_2)_{0.8(1+R)}$ glasses obtained from the experimental values in Fig. 10(b) (Ref. 48).

different regions of the "β versus E_a" curve shown in Fig. 8(a). As we have noted, the curvature of this relationship decreases for smaller E_a values and accordingly leads to a smaller rise in $\beta_{Na/K}$ between $\gamma=0,1$ and $\gamma\approx0.5$ for $R=1$ compared to $R=0$ compositions. Through Eqs. (6) and (15) we can see that this will result in a proportionately larger overall increase in the dc electrical conductivity activation enthalpy ΔW for $R=1$ compared to $R=0$ glasses. The origin of this behavior is indeed due to the removal of NBO's from the glass structure, but as we have argued, this change in structure should be reflected in the progressive removal of the conformational energy ΔE_i of each alkali from the respective primitive diffusion enthalpy E_{ai} [Eqs. (5) and (12)]. By reducing E_{ai} through adding alumina to the composition in place of silica, more cooperativity is engaged for each of the alkalis present and the working range of "β versus E_a" in Fig. 8(a) relevant to the mixed-alkali effect travels to the left. The change in β_i for a given change in E_{ai} is therefore smaller for either alkali, ensuring a more pronounced ΔW versus γ characteristic as we see in Fig. 17.

X. CONCLUSIONS

In this account of glass structure and alkali transport, we have stressed the relationship between the microsegregation of alkalis, nearest-neighbor hopping, cooperative, and correlation effects. MRN and CCRN structures offer simple ways of visualizing this and of determining the degree of participation of NBO's in alkali diffusion. In particular, we have shown how the local structure information from XAFS and MASNMR for sodium and potassium oxide glasses together with the value for ε_{hf}, the high-frequency dielectric constant, can be used to calculate the microscopic energy barrier E_a facing a migrating alkali. By combining this with the results of electrical conductivity relaxation, which yield values for the Kohlrausch exponent β, we have been able to predict with considerable accuracy the macroscopic activation enthalpy for diffusion, W, for sodium and potassium by exploiting the relation $W=E_a/\beta$. Moreover, by utilizing the results of far-IR spectroscopy together with the glass composition, the preexponents D_0 and $(\sigma_{dc}T)_0$ for diffusion and dc electrical conductivity can also be accurately estimated, not just in these alkali silicates, but also in aluminosilicate glasses. Throughout we stress the facility of employing the empirical relationship between "β and E_a" and also one connecting the Haven ratio f with E_a in order to obtain values for β and f from local structure where these are not known for a particular glass.

Decreasing the concentration of sodium or potassium, x, in a glass from stable glass compositions ($0.2<x<0.3$) globally leads to smaller values of the high-frequency dielectric constant ε_{hf}. At the microstructural level, we expect this reduction in alkali content to result in the gradual disappearance of microsegregation and with it a reduction in cooperative effects in alkali migration, accompanied by increases in average hopping distances $R_{M\text{-}M}$ and in the hopping attempt frequency ν_0. Account is also taken of the "β versus E_a" relation, which points up the progressive phasing out of coopera-

tive ionic behavior as x falls. The corresponding relationship between the Haven ratio f and E_a highlights the reduction in nonrandom ionic migration that accompanies increasing E_a. All of these things taken together explain the rises in W and D_0 and also β and f reported from alkali transport experiments in oxide glasses as x is lowered.

In mixed-alkali glasses, on the other hand, the structure, ε_{hf}, and ν_0 scarcely change with γ for a given x, and so the increases in W and D_0 observed as the proportion of a given alkali is decreased are attributed to increases in $R_{M\text{-}M}$. In this way, the characteristic "crossover" behavior of the diffusion coefficients and enthalpies of sodium and potassium can be convincingly reproduced for mixed-alkali silicates. We show how this infers separate β values for each alkali and an equivalent "crossover" as alkalis are mixed. Again, we make use of the experimental "β versus E_a" relationship to parametrize the decreased cooperative motion of the minority alkali at the expense of the majority alkali, which also quantitatively reproduces the rise in β which accompanies the increase in the electrical conductivity enthalpy W_{dc} observed as γ approaches 0.5. In a similar way the "f versus E_a" relationship leads to a crossover in the f values of the two alkalis and to the maximum in f reported for ionic transport in mixed-alkali glasses. The absolute magnitude of the dc electrical conductivity and diffusivity isotherms are also well reproduced in sodium-potassium silicates and in aluminsilicate glasses too, where the magnitude of the effect increases as $R \Longrightarrow 1$. We have shown how the latter phenomenon results naturally from the increased cooperativity expected as E_a is reduced by the removal of NBO's.

We believe that our empirical approach, which unifies the results of structure, electrical conductivity relaxation, and ionic diffusion in simple binary and ternary oxide glasses, has more general application. In particular, what we have demonstrated for single- and mixed-sodium-potassium-alkali silicate and aluminosilicate glasses will also be relevant where other alkali combinations are concerned. The ideas laid out in this paper should also help in understanding the structural origin of ionic transport for more complicated glass compositions, for instance, where more than two alkalis are present in a glass or where one alkali is replaced by an alkaline earth or where other glass formers like B_2O_3 or P_2O_5 are employed.

ACKNOWLEDGMENTS

G.N.G. is supported by the Council for the Central Laboratory. K.L.N. is supported in part by ONR Contract No. N0001494 WX23010.

[1]J. O. Isard, J. Non-Cryst. Solids **1**, 235 (1969); D. E. Day, *ibid.* **21**, 343 (1976).
[2]W. H. Zachariasen, J. Am. Chem. Soc. **54**, 3841 (1932).
[3]G. N. Greaves, A. Fontaine, P. Lagarde, D. Raoux, and S. J. Gurman, Nature (London) **293**, 611 (1981).
[4]G. N. Greaves, in *Glass Science and Technology,* edited by D. R. Uhlmann and N. J. Kreidl (Academic, London, 1990), Vol. 4A, p. 1.
[5]S. N. Houde-Walter, J. M. Inman, A. J. Dent, and G. N. Greaves, J. Phys. Chem. **97**, 9330 (1993).
[6]R. Dupree, D. Holland, and M. G. Mortuza, J. Non-Cryst. Solids **116**, 148 (1990).
[7]H. Maekawa, T. Maekawa, A. Kawamura, and T. Yokakawa, J. Non-Cryst. Solids **127**, 53 (1991).
[8]W. Hater, W. Müller-Warmuth, M. Meier, and G. H. Frischat, J. Non-Cryst. Solids **113**, 210 (1989).
[9]I. Farnan, P. J. Grandinetti, J. H. Baltisberger, J. F. Stebbins, U. Werner, M. A. Eastman, and A. Pines, Nature (London) **358**, 21 (1992).
[10]P. H. Gaskell, in *The Physics of Non-Crystalline Solids,* edited by L. D. Pye, W. C. LaCourse, and H. J. Stevens (Taylor & Francis, London, 1992), p. 15.
[11]E. I. Kamitsos, A. P. Patsis, and G. D. Chryssikos, in *The Physics of Non-Crystalline Solids,* edited by L. D. Pye, W. C. LaCourse, and H. J. Stevens (Taylor & Francis, London, 1992), p. 461.
[12]N. Umesaki, N. Iwamoto, M. Tatsumisago, and T. Minami, J. Non-Cryst. Solids **106**, 77 (1988).
[13]R. Brückner, H. U. Chum, H. Goretzki, and M. Sammet, J. Non-Cryst. Solids **42**, 49 (1980).
[14]D. Sprenger, H. Bach, W. Meisel, and P. Gütlich, J. Non-Cryst. Solids **159**, 187 (1993).
[15]C. Huang and A. N. Cormack, J. Chem. Phys. **93**, 8180 (1990).
[16]C. Huang and A. N. Cormack, J. Chem. Phys. **95**, 3634 (1991).
[17]B. Vessal, G. N. Greaves, P. T. Martin, A. V. Chadwick, R. Mole, and S. Houde-Walter, Nature (London) **356**, 504 (1992).
[18]C. Huang and A. N. Cormack, J. Mater. Chem. **2**, 281 (1992).
[19]G. N. Greaves, J. Non-Cryst. Solids **71**, 203 (1985).
[20]G. N. Greaves and K. L. Ngai, in *Proceedings of the International Conference on Defects in Insulating Materials,* edited by O. Kanert and M. Spaeth (World Scientific, Singapore, 1993), p. 53.
[21]A. N. Cormack (private communication).
[22]K. L. Ngai and S. W. Martin, Phys. Rev. B **40**, 10 550 (1989).
[23]G. N. Greaves, C. R. A. Catlow, B. Vessal, J. Charnock, C. M. B. Henderson, R. Zhu, S. Wang, S. J. Gurman, and S. Houde-Walter, in *New Materials and their Applications 1990,* Proceedings of the 2nd International Symposium on New Materials and their Applications, edited by D. Holland, IOP Conf. Proc. No. 111 (Institute of Physics and Physical Society, London, 1990), p. 411.
[24]G. H. Frischat, in *Ionic Diffusion in Oxide Glasses* (Trans. Tech., Aedermannsdorf, 1975).
[25]P. B. Macedo, L. P. Moynihan, and R. Bose, Phys. Chem. Glasses **13**, 171 (1972); J. M. Hyde, M. Tomozawa, and M. Yoshiyagawa, *ibid.* **28**, 174 (1987).
[26]S. J. Gurman, J. Non-Cryst. Solids **125**, 151 (1990).
[27]Y. Cao and A. N. Cormack (private communication).
[28]C. T. Moynihan, L. P. Boesch, and N. L. Laberge, Phys. Chem. Glasses **14**, 122 (1973).
[29]S. W. Martin and C. A. Angell, J. Non-Cryst. Solids **83**, 185 (1986).
[30]J.-P. Bouchard and A. Georges, Phys. Rep. **4-5**, 127 (1990).
[31]C. A. Angell, Chem. Rev. **90**, 523 (1990).
[32]C. A. Angell, Annu. Rev. Phys. Chem. **172**, 1 (1992).
[33]K. L. Ngai, J. Chem. Phys. **98**, 6424 (1993).

[34]K. L. Ngai, Phys. Rev. B **48**, 13 481 (1993).
[35]P. Maass, J. Petersen, A. Bunde, W. Dieterich, and H. E. Roman, Phys. Rev. Lett. **66**, 52 (1991).
[36]A. Bunde, P. Maass, and M. Meyer, in *Proceedings of the International Conference on Defects in Insulating Materials,* edited by O. Kanert and M. Spaeth (World Scientific, Singapore, 1993), p. 295.
[37]K. Funke, Prog. Solid State Chem. **22**, 111 (1993).
[38]K. L. Ngai and O. Kanert, Solid State Ion. **53-56**, 936 (1992); K. L. Ngai, J. Phys. (France) IV Colloq. **2**, C2-61 (1992).
[39]K. L. Ngai, in *Disorder Effects in Relaxation Processes,* edited by R. Richert and A. Blumen (Springer-Verlag, Berlin, 1994).
[40]K. L. Ngai, Comments Solid State Phys. **9**, 127 (1991).
[41]K. L. Ngai, S. L. Peng, and K. Y. Tsang, Physica A **191**, 523 (1992); K. L. Ngai and G. N. Greaves, in *Diffusion in Amorphous Materials,* edited by H. Jain and D. Gupta (TMS, Warrendale, PA, 1994); K. L. Ngai, M. Roland, and G. N. Greaves, J. Non-Cryst. Solids **182**, 172 (1995); K. Y. Tsang and K. L. Ngai, Phys. Rev. E (to be published).
[42]G. Balzer-Jöllenbeck, O. Kanert, H. Jain, and K. L. Ngai, Phys. Rev. B **39**, 6071 (1989).
[43]In an earlier publication (Ref. 20), we employed the expression for diffusion enthalpy, $W=e^2/4\pi\varepsilon_0\varepsilon_{\rm hf}[1/R_{M\text{-}O}-1/R_{M\text{-}M}]/\beta+\Delta E_{R=0}$, rather than $W=e^2/4\pi\varepsilon_0\varepsilon_{\rm hf}[1/R_{M\text{-}O}-1/R_{M\text{-}M}]/\beta+\Delta E_{R=0}/\beta$ given by Eqs. (4) and (6). It is clear, however, that the conformational energy term $\Delta E_{R=0}$, which we attribute to local disproportionation, is also part of the cooperative motion of the alkalis and should therefore be scaled by $1/\beta$ along with the Coulomb contribution.
[44]R. D. Williams and S. R. Elliott, J. Non-Cryst. Solids **146**, 43 (1992); F. Ali, A. V. Chadwick, G. N. Greaves, M. C. Jermy, K. L. Ngai, and M. E. Smith (unpublished).
[45]J. E. Kelly III, J. F. Codaro, and M. Tomazawa, J. Non-Cryst. Solids **41**, 47 (1980).
[46]C.T. Moynihan, N. S. Saad, D. C. Tranand, and A. V. Lesikar, J. Am. Ceram. Soc. **63**, 458 (1980).
[47]A. K. Varsheyna, J. Am. Ceram. Soc. **57**, 37 (1974).
[48]J. C. Lapp and J. E. Shelby, J. Non-Cryst. Solids **95&96**, 889 (1987).
[49]J. W. Flemming and D. E. Day, J. Am. Ceram. Soc. **55**, 186 (1972).
[50]H. Jain, N. L. Peterson, and H. L. Dowing, J. Non-Cryst. Solids **55**, 283 (1983).
[51]P. Maass, A. Bunde, and M. D. Ingram, Phys. Rev. Lett. **68**, 3064 (1992).
[52]H. Kahnt and J. M. Reau, J. Non-Cryst. Solids **125**, 143 (1990).
[53]M. D. Ingram, M. A. Mackenzie, W. Muller, and M. Torge, Solid State Ion. **28-30**, 677 (1988).
[54]S. Kirkpatrick, Rev. Mod. Phys. **45**, 574 (1973).
[55]J. M. Hyde, M. Tomozawa, and M. Yoshiyagawa, Phys. Chem. Glasses **28**, 174 (1987).
[56]A. O. Ivanov, Sov. Phys. Solid State **5**, 1933 (1964).
[57]W. A. LaCourse, in *The Physics of Non-Crystalline Solids,* edited by L. D. Pye, W. C. LaCourse, and H. J. Stevens (Tay-